UNIVERSITY OF CALIFORNIA, SAN DIEGO

Probing Structural Features of Amyloid-Beta Ion Channels in Membranes Using A-Beta Mutants

A thesis submitted in partial satisfaction of the requirements
for the degree Master of Science

in

Engineering Sciences (Mechanical Engineering)

by

Samuel Aaron Kotler

Committee in Charge:

Professor Ratnesh Lal, Chair
Professor Alison Marsden
Professor Jerry Yang

2011

The Thesis of Samuel Aaron Kotler is approved, and it is acceptable in Quality and form for publication on microfilm and electronically:

_____

_____

_____

Chair

University of California, San Diego

2011

TABLE OF CONTENTS

LIST OF FIGURES

ACKNOWLEDGEMENTS

I would like to acknowledge and thank Professor Ratnesh Lal for his support as my advisor and chair of my committee. He gave me the extraordinary opportunity to work in a laboratory with the experience and knowledge to succeed.

I would like to acknowledge and thank Ricardo Capone for his brilliant mentorship and guidance. His thorough training, persistence, and friendship are deeply appreciated. I would also like to thank the rest of the members of Professor Lal's lab for all of their support and good humor.

Finally, I would like to acknowledge Professor Alison Marsden and Professor Jerry Yang for their willingness to be on my committee and provide valuable advice.

The material in the Results and Discussion (chapter 3), in part are currently being prepared for submission for publication: Lal, Ratnesh; Capone, Ricardo; Kotler, Samuel

Funded by extramural NIH-NIA Program number 7R01AG028709-06 (Lal, Ratnesh).

ABSTRACT OF THE THESIS

Probing Structural Features of Amyloid-Beta Ion Channels
in Membranes Using A-Beta Mutants

by

Samuel Aaron Kotler

Master of Science in Mechanical Engineering

University of California, San Diego, 2011

Professor Ratnesh Lal, Chair

A current hypothesis for the pathology of Alzheimer's disease (AD) proposes that amyloid-beta (Aβ) peptides induce uncontrolled, neurotoxic ion flux across cellular membranes. The resulting inability of neurons to regulate their intracellular concentration of ions, in particular calcium ions, has been associated with cell death and may thus contribute to cognitive impairment typical for AD. The mechanism of the ion flux is not

fully understood since no experimentally based Aβ channel structures at atomic resolution are currently available, and few polymorphisms have been predicted by computational models. Structural models and experimental evidence suggest that Aβ channel is an assembly of loosely-associated mobile β-sheet subunits. Using planar lipid bilayers, we present a study showing that amino acidic substitutions can be used to infer which residues are essential for channel structure and/or line the pore. We tested: Aβ42-F19P, Aβ42-F20C, Aβ42-A42C, and Aβ42-D1C. The substitution of F19P inhibited channel formation. All the cysteine mutants tested are capable of forming channels, but with different characteristics. This and other structural information on or in membrane are needed to aid the understanding of channel formation and structure. Additionally, this information should aid studies of drug design aiming to control unregulated Aβ ion fluxes.

1. INTRODUCTION

1.1 Amyloids and Alzheimer's Disease

The increase in life expectancy in the modern era has increased the portion of the population subject to neurodegenerative diseases occurring late in life [1-3]. It is now known that most patients of Western societies experiencing intellectual failure during old age results from the progressive degeneration of neurons [3]. In the last 20 years studies indicated that amyloid deposits characterize at least 16 different clinical syndromes, each of which are associated with a distinct amyloid protein [4-6]. Amyloid proteins have been the topic of research for over a century. In the mid-nineteenth century Rudolph Virchow mistakenly described amyloids as starch-like, carbohydrate deposits that stained purple when exposed to iodine [4-8]. Subsequent studies found that these deposits were composed of proteins [9]. Any disease distinguished by the extracellular deposition (fibrils) of an amyloid protein is referred to as amyloidosis [10, 11]. Well-known neurodegenerative diseases such as Alzheimer's Parkinson's, and Huntington's diseases, as well as systemic diseases like amyloid light chain (AL) amyloidosis and localized diseases like type II diabetes are believed to be induced by the aggregation and misfolding of amyloidogenic peptides [4-6, 12-27]. Of these amyloid related diseases, Alzheimer's disease (AD) is the most known and socially distressing; affecting 5.4 million people in the United States and more than 24 million people worldwide [24, 28-30].

AD is clinically characterized by the presence of intracellular neurofibrillary tangles and extracellular senile plaques [4-6, 12-28]. These plaques are insoluble amyloid deposits composed primarily, but not only, of aggregates of amyloid-beta (Aβ) in their

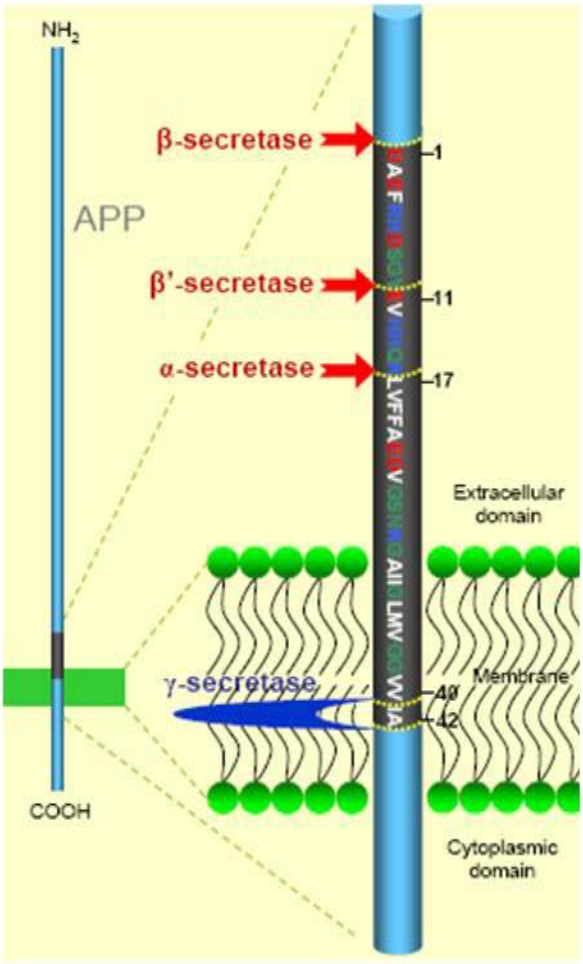

Figure 1: Amyloid β formation. Representation of the cleavage process of amyloid precursor protein (APP) by α-, β-, and γ-secretase. Various Aβ fragments are processed by different secretase combintaions. Amyloidogenic fragments of Aβ40/Aβ42 are produced by β- and γ-secretase cleavage. From Thinakaran et al 2008 and Jang et al 2010, modified [14, 31].

fibril form. The Aβ peptide is derived from the amyloid precursor protein (APP). APP is processed by many enzymes, but Aβ is specifically processed by the enzymes β- and γ-secretase (see figure 1) [25, 32, 33]. These secretases cleave APP to produce the Aβ peptide, predominantly the species Aβ40 and Aβ42 peptides (consisting of 40 and 42

residues, respectively) [1, 23, 25, 32-34]. Although Aβ is found in large fibrils in the brain, the mechanism by which Aβ causes neurotoxicity is not fully understood. The etiology of AD is under intense debate and one prevailing hypothesis is the "amyloid hypothesis" [1-6, 9, 12-21, 34-50]. The amyloid hypothesis states that Aβ is the toxic agent in AD pathology [51]. Previous research pointed to Aβ fibrils (see figure 2) specifically as the neurotoxic agent leading to cellular death, memory loss, and other AD characteristics. A great body of research has studied the biological effects and structural aspects of Aβ fibrils [52-59]. This data has been correlated with brain samples from patients with and without AD (see figure 3) [29, 30]. To this day, the Aβ fibrils define and confirm the diagnosis of AD patients' post-mortem [24, 29].

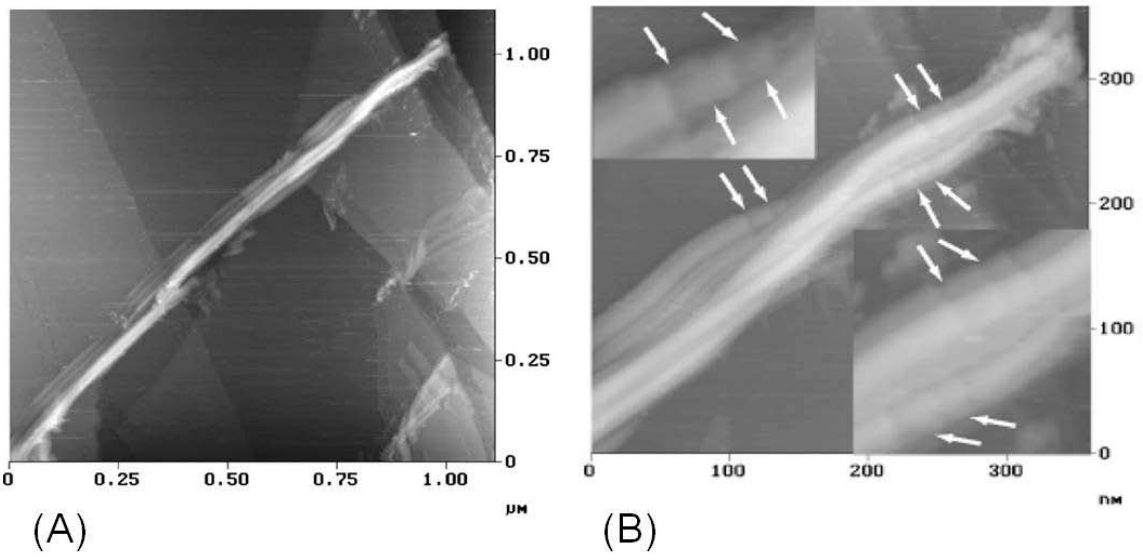

Figure 2: Aβ forms fibers. Scanning Tunneling Microscopy images of an Aβ fibril with a right-handed twist taken from Wang et al 2003 [59]. (A) Mature Aβ fibril with a length of about 1 μm and width of 8-14 nm. Wang et al 2003 suggest that nucleation of the fibril occurred on the edge of several graphite layers or in liquid during the sample's incubation period. (B) High-resolution image of the Aβ fibril. The arrows point out locations of periodicity 12-18 nm long, suggesting that the fibrillization of Aβ is an association process of monomers and protofibrils.

During the last 18 years, a minority view in the community of AD research suggested that fibrils were not the predominant neuro-toxic agent in AD. Today, the fibrils are no longer considered the main toxic agent in AD, but rather oligomers of the Aβ species have been shown to be most damaging to cells [21, 60-65]. On the way to fibril formation, Aβ monomers either associate directly to fibers or aggregate among them to generate various sized oligomers (e.g. dimers, trimers, tetramers, etc.) eventually leading to fibers. Thermodynamically, aggregated states of Aβ have lower free energy, fibers being the state with the lowest free energy and the most stable. Thus, the Aβ peptide prefers aggregation; however, the most toxic species are the oligomeric states [20, 21, 40, 43, 64, 65]. The research of Aβ's development from oligomers to fibrils is ongoing and the unstable nature of oligomeric structures complicates efforts aimed at characterizing the Aβ toxic species [1-4, 6].

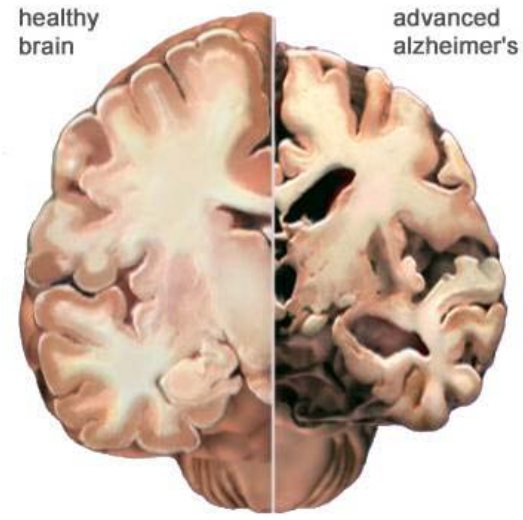

Figure 3: Effects of Alzheimer's on human brain [30]. Image depicting a healthy human brain vs. a human brain in the advanced stages of Alzheimer's disease. In the Alzheimer's brain the cortex deteriorates causing neuronal damage to areas of the brain involved in thinking, planning, and memory. Specifically

within the cortex, the hippocampus suffers a reduction in mass, a part of the brain playing a key role in formation of new memories.

The aggregation of Aβ monomers into various oligomers is further hampered by the extreme sensitivity to a multitude of factors [52, 66-68]. Aβ aggregation is a nucleation dependent process and fibril formation can depend on seed-type. Additionally, Aβ aggregation is contingent on parameters such as pH, ionic strength, and presence of solvents [48, 49, 52, 53, 69]. The outcome of the aggregation is heavily biased by the presence of "seeding elements" [66-69]. This fact focused research on finding conditions that would allow "seedless" preparations [70]. Due to these experimental difficulties, information about Aβ aggregation onto and into model or cellular membranes is unclear.

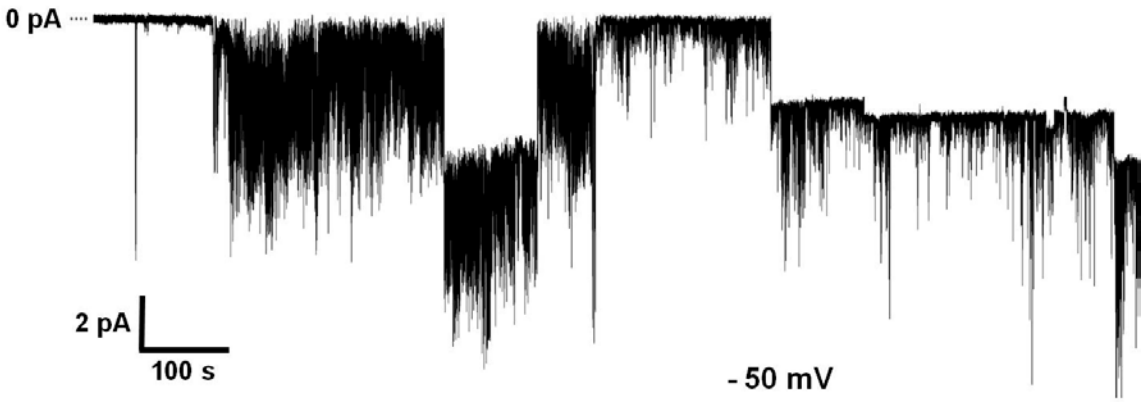

Figure 4**:** Current vs. time trace of Aβ42 wild type (Aβ42-WT) channel activity. The activity seen here shows the typical behavior for the Aβ peptide: spikes, bursts, and steps. The activity was well sustained with fast openings and closings, along with sustained steps in current jumps. The trace was recorded at -50 mV of applied potential. Aqueous solution used contained 150 mM KCl, 10 mM Hepes pH 7.4, and 1 mM $MgCl_2$. The bilayer was composed of 1:1 w/w DOPS:POPE, and was done by the painted technique.

In order to be cytotoxic, Aβ aggregates must interact with the cellular surface by either a receptor or the membrane itself [1, 3, 4, 6, 23, 34, 51]. Interaction(s) with the

membrane is likely to affect the structure and properties of any type of aggregate or oligomer. One mechanism of interaction suggests that Aβ is cytotoxic due to its ability to form ion channels, inducing an unregulated ion flux across cellular membranes [13, 27, 40-43, 47, 49, 50, 71]. The ionic fluxes produced by Aβ channels create a state of dyshomeostasis of calcium ions, leading to cell death. Understanding the molecular mechanics by which Aβ induces ionic flux has become crucial to AD pathology. The cellular membrane in live cells is very complex involving many variables which are very difficult to isolate and control. Consequently, studying the ionic flux across a cellular membrane due to specific membrane proteins is extremely challenging. As a result, we examine ionic flux across model bilayers by imploring specific techniques to make planar lipid bilayers (PLB). By using a model membrane we ensure a pure system that isolates specific membrane permeabilizing peptides. Aβ40 and Aβ42 have been shown to exhibit channel-like activity in artificial bilayers (PLBs). This activity is a result of ionic flux and is unfavorable since it shows a wide range of heterogeneous conductances. The activity is not fully dependent on the concentration of Aβ species, suggesting that a subset of the possible structures is required to obtain channel activity. Ionic fluxes resulting from Aβ permeabilization has been shown to be inhibited by metal ions such as Zn^{2+} [49]. An example of an unusually long current trace showing activity of Aβ42 is depicted in figure 4.

1.2 Modeling Amyloid-β Ion Channels

Due to the inability to crystallize stable and homogeneous Aβ preparations on membranes, the use of computational techniques to model Aβ structure in membranes has

become predominant [13, 14, 44, 72-77]. Robert Guy and co-workers developed the first model(s) for Aβ channels [44]. In that work, they proposed that Aβ40 peptide forms a β-hairpin followed by a helix-turn-helix motif. Durell and co-workers developed three different models of Aβ channels, centered on the aforementioned motif, which were distinguished by whether the pore was formed by the β-hairpin, the middle helices, or the hydrophobic C-terminus [44]. To our knowledge, this was the only study of theoretical models for Aβ channel structures until 2010.

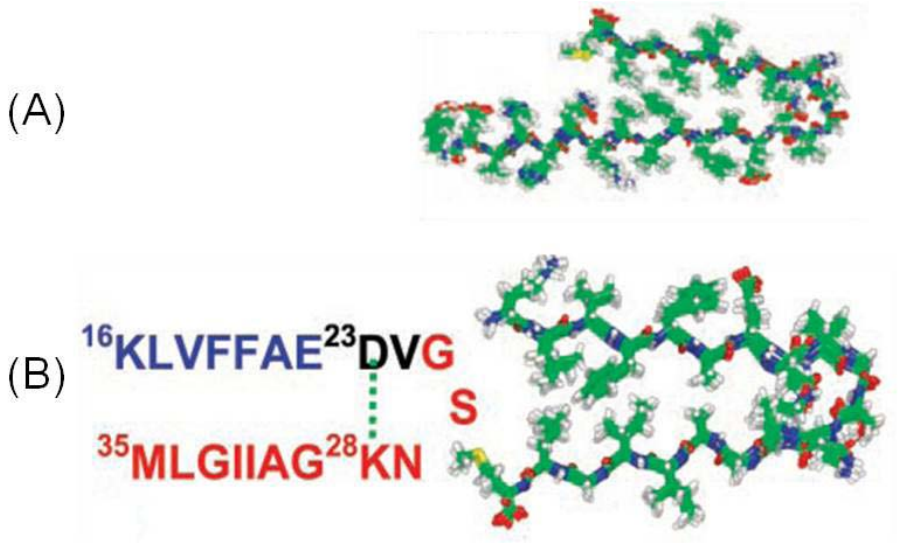

Figure 5: The U-turn model of amyloids. Illustration of β-strand arrangement for (A) Aβ10-35 and (B) Aβ16-35 taken from Ma et al 2002 [76]. Both models show a parallel β-sheet with a bent hair-pin conformation. To the best of our knowledge this was the first model demonstrating the U-turn motif for the Aβ peptide.

In 2002, the laboratory of Ruth Nussinov developed a model of an Aβ fragment based on solid state NMR experiments done by the laboratory of Robert Tycko [58, 76, 78]. In Balbach et al 2000 [58], they showed that the Aβ16-22 fragment forms highly ordered fibrils upon incubation in aqueous solutions and further indicated a β-strand

conformation of the peptide backbone centered at the phenylalanines (F19 and F20). From these coordinates, Nussinov and co-workers simulated Aβ16-22 and proposed that an antiparallel β-sheet orientation was the most stable conformation for this shorter fragment [76]. Simulations were also done for the longer fragments Aβ16-35 and Aβ10-35 [76], proposing a parallel β-sheet structure (see figure 5) as solid-state NMR indicated parallel organization within the sheet [76, 79, 80]. The simulations presented by Ma et al 2002 revealed the underlying mechanism of the parallel organization for these longer, soluble Aβ fragments. This group has helped universalize the U-turn motif into other amyloid and amyloid-like peptides such as K3 , Aβ17-42 (p3), and PG-1. [12-14, 18, 39].

In recent years several models have been proposed for Aβ channels and its inherent variability. In general, the models of Aβ channels suggest that almost all of the hydrophobic groups in Aβ are exposed to the hydrophobic hydrocarbon chains of the plasma membrane, groups of polar atoms in Aβ are exposed to water or form hydrogen bonds, and that most charged groups of Aβ are in or near the pore and assist binding to ions of opposite charge [72]. Furthermore, the models of Aβ channels suggest a β-sheet rich structure for the Aβ peptide

Recently, Guy and co-workers revisited their models of Aβ channels. Shafrir et al 2010 used molecular dynamics (MD) simulations to present a study favoring an antiparallel β-barrel (a closed-form structure of β-sheet) model of Aβ oligomers (figure 6) [74]. The central hypothesis for these models is that the hydrophobic C-terminus assembles to form a six-stranded β-barrel, maintaining “exceptional stability”. The models of the Aβ channels presented in their latest study (see figure 6) began with hexamers and built up to 36-mers [73, 74]. The recent models of soluble and membrane-

bound Aβ oligomers presented by Guy and co-workers align with NMR and other results and hold that the hydrophilic segment (Aβ1-16) is the least ordered in solution and the hydrophobic segment (Aβ22-42) is the least ambiguous.

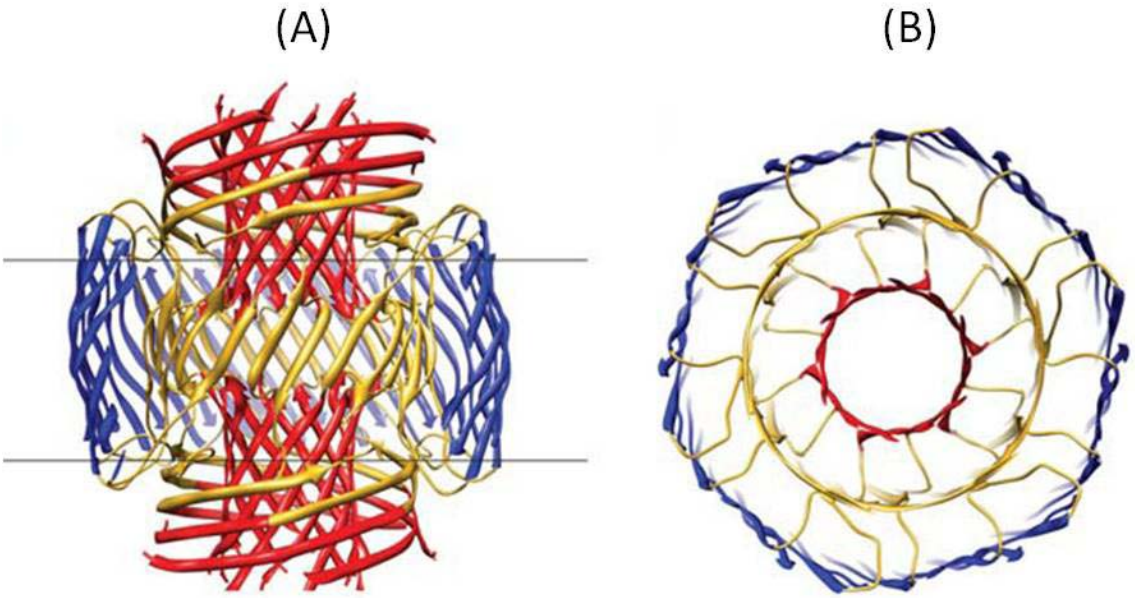

Figure 6: Aβ model from the Guy laboratory. A conformation of an Aβ42 36-strand antiparallel β-barrel proposed in Shafrir et al 2010 [73]. The color scheme divides the Aβ42 monomer into 3 segments: red is residues 1-14, yellow is residues 15-28, and blue is residues 29-42. (A) Side-view of the complete model. The black lines approximate the boundary of the membrane's hydrophobic core. (B) Top view of half the model.

The Nussinov group has expanded on their previous models of Aβ fragments and extended their work to models of Aβ channel structures. They propose a model of a monomeric state of Aβ with a β-strand-turn-β-strand motif (i.e. the concept that residues 17-42 form a U-turn, see figure 7) [14] and a disorganized mobile component (residues 1-16) [81]. The simulation shown in figure 7 began with a circular assembly of Aβ structures in the membrane that, over time, formed channel-like structures composed of a

varying number of subunits (a subunit being oligomers with 3-6 monomers). The subunits appear to be mobile and could move in and out of the channel structure [14].

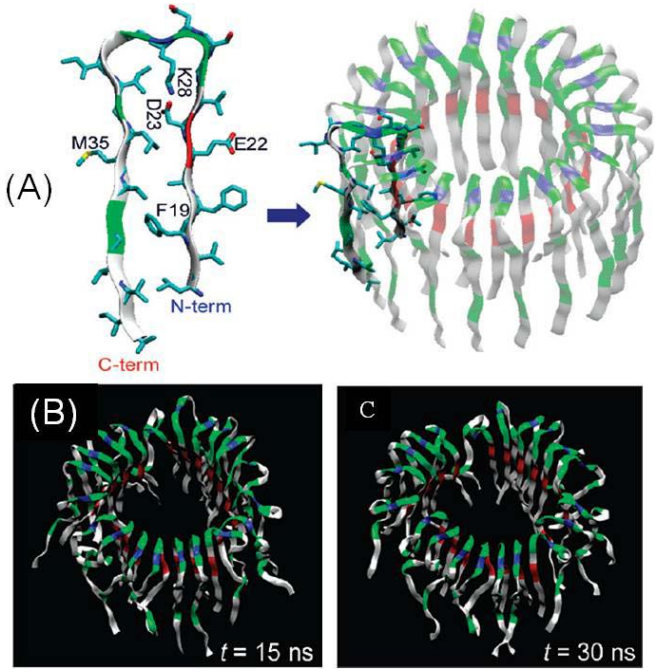

Figure 7: Aβ17-42 channel model from the Nussinov laboratory. MD model of Aβ annular channel structure taken from Jang et al 2010 [14]. (A) This particular model was assembled from a circular arrangement of monomers the Aβ17-42 fragment (p3) with the U-turn motif embedded in lipid bilayer. Note that the two residues colored red (E22 and D23) are negatively charged and line the inner channel structure, suggesting a pore that is cation selective. The annular channel structure represents the starting point for the simulation in a DOPC bilayer (time t=0 ns). Snapshots of the Aβ17-42 channel were taken at time (B) t=15 ns and (C) t=30 ns. The channel structures relax in the bilayer over time and formation of subunits can be observed.

This model fits well with data acquired by atomic force microscopy (AFM) and electron microscopy (EM). Furthermore, electrical recordings involving planar lipid bilayers (PLB, the technique used in this thesis) supports the idea of mobile subunits given the measured heterogeneous conductance of Aβ ion channel formations [13, 14, 16, 17, 75, 76]. The latest MD model presented by the Nussinov group at the 2011 Biophysical Society Meeting expands on their previous model and proposes a β-barrel conformation comprised of the full length Aβ42 monomers embedded in a membrane similar to the

model proposed for Aβ17-42 (Hyunbum Jang, personal communication). Figure 8 shows the starting point for these MD simulations. This work is currently being prepared for publication.

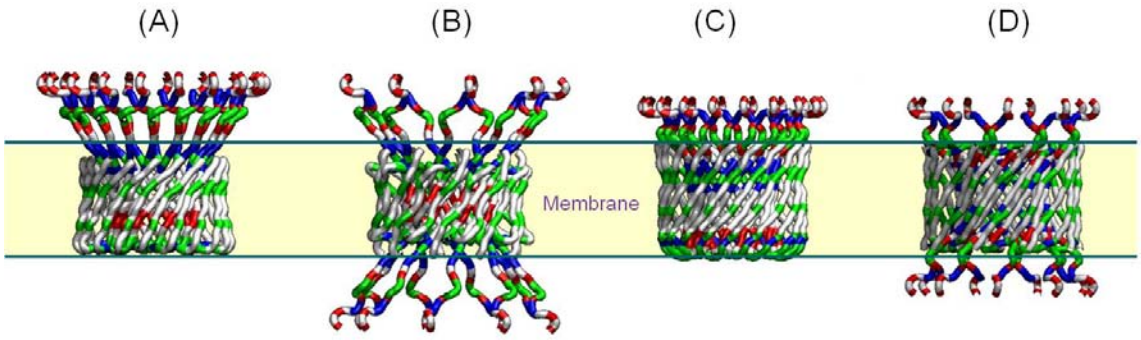

Figure 8: Aβ42 channel model from Nussinov laboratory. Starting point for MD β-strand barrel models of Aβ42 channel structures for two known monomer polymorphisms. (A) Parallel β-strand barrel with turn between residues S26-I31. (B) Antiparallel β-strand barrel with turn between residues S26-I31. (C) Parallel β-strand barrel with turn between residues D23-G29 turn. (D) Antiparallel β-strand barrel with turn between residues D23-G29. Each model depicts its respective conformation at time t=0 ns. The manuscript for the time-elapsed models of these conformations is in preparation (Hyunbum Jang, personal communication).

A variation similar to the Nussinov U-turn motif was proposed by Strodel et al 2010 using a different simulation technique (see figure 9) [77]. The focus of this work was to predict the structure of the full length Aβ42 peptide in membrane. Using a global optimization approach, they suggested an oligomeric structure that is inserted into the hydrophobic core of the membrane between residues 17-42 (much like the p3 model from the Nussinov group). The structure spanning the membrane displayed a similar β-strand-turn-β-strand motif as observed in NMR experiments; however, Strodel et al [77] predicted an additional strand-turn-strand motif between residues M35 and A42 for the monomers (see figure 9). Strodel et al suggested that these monomers form ordered oligomeric structures, leading to Aβ pores that consist of β-sheet subunits. Remarkably,

using a different approach, Strodel and co-workers reached very similar conclusions to those previously proposed by Nussinov and co-workers with the U-turn model of the Aβ17-42 channel.

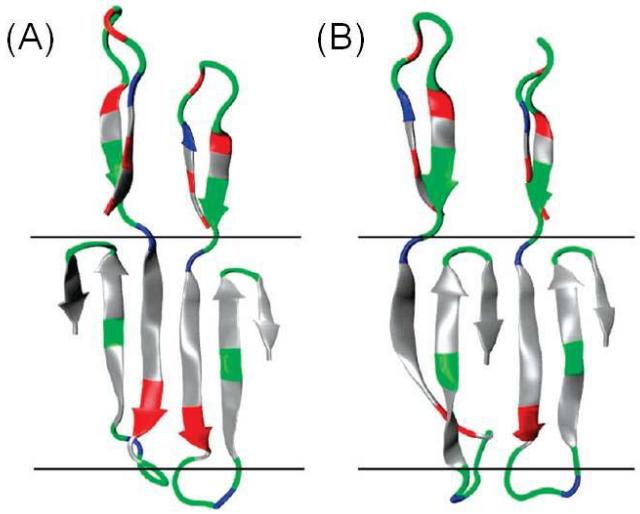

Figure 9: Aβ42 dimer model from Strodel et al [77]. Dimer structures of Aβ42 forming an alternative U-turn-like motif. The residues are color coded according to physiochemical properties: blue is basic, red is acidic, gray is hydrophobic, and green is polar. The black lines indicate the boudary of the hydrophobic core of the lipid bilayer (i.e. the hydrocarbon chains). (A) The N-terminal regions of the Aβ42 dimer form an interface and the C-terminal regions point outward, whereas in (B) the C-terminal region of the first peptide forms a β-sheet with the N-terminal region of the second peptide

While there are a number of models suggesting different conformations of Aβ channels, this work will focus on experimentally tested channel formations by Aβ42 as increasing evidence points to oligomers rich with β-sheet structure as the species toxic to neurons. Structural models of Aβ channels, such as the ones described above, help propose testable experiments which, in turn, provides further insight to optimize these models.

1.3 Using Amyloid-β Mutants to Understand Channel Structure

The goal of this thesis was to test selected Aβ42 amino acidic substitutions for Aβ-channel activity to gain information on the structural requirements for Aβ channel formation and structure. In the choice of the specific substitutions, we guided ourselves with the proposed models of Aβ channels and other structural information regarding Aβ conformations.

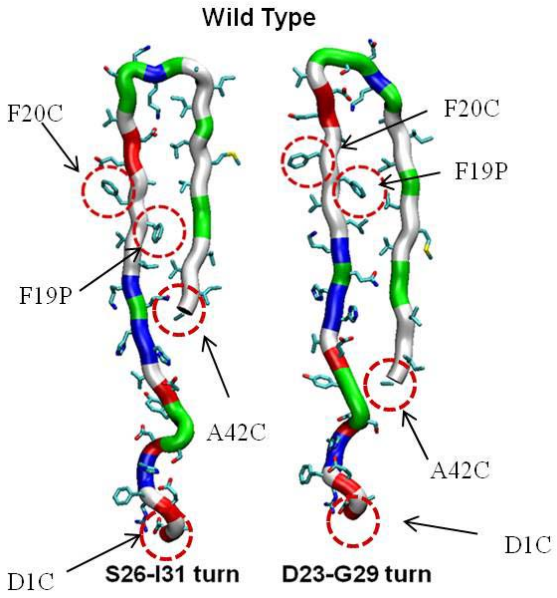

Figure 10: Structural polymorphisms of Aβ42 monomers with U-turn motif [81]. MD models of the Aβ42 monomer with U-turn motif. (A) Aβ42 monomer with turn from S26 to I31 and (B) with turn from D23 to G29. The regions circled in red indicate the four locations where we made point mutations in the Aβ42 peptide sequence: D1C, F19P, F20C, and A42C. The manuscript for this image is in preparation (Hyunbum Jang, personal communication).

Our results help validate and/or improve the proposed models. The results gathered are used to understand the structure(s) of the Aβ channel and its requirement for formation. Aβ oligomers are believed to cause an imbalance in ionic homeostasis via ion channel-like pores [15-17, 19-21, 40-43, 48, 49]. Using planar lipid bilayers (PLB) we

study the ability of Aβ42 mutants to form ion channels in model membranes. The aim is to understand which residues are structurally necessary, line the pore, and whether those residues are water accessible. The work described here presents preliminary studies of the first set of mutants: Aβ42-F19P, Aβ42-F20C, Aβ42-A42C, and Aβ42-D1C (highlighted in figure 10). Figure 10 depicts the two Aβ42 polymorphisms that were used as a starting point in the MD models from the Nussinov β-strand barrels shown in figure 8 (each of which has turns at different locations as described in the caption). This and other structural information on or in membrane are needed to map channel structure(s) and aid drug design seeking to control unregulated Aβ ion fluxes.

2. MATERIALS AND METHODS

2.1 Materials

We purchased Aβ42-wild type, Aβ42-F19P, Aβ42-F20C, Aβ42-A42C, and Aβ42-D1C from Bachem Inc. and we purchased all phospholipids from Avanti Polar Lipids, specifically: 1,2-dioleoyl-*sn*-glycero-3-phosphoserine (DOPS) and 1,2-dioleoyl-*sn*-glycero-3-phosphoethanolamine (DOPE). All other chemicals were purchased from Sigma-Aldrich.

2.2 Formation of Planar Lipid Bilayers

We prepared planar lipid bilayers (also called black lipid membranes or bilayer lipid membranes (BLM)) by using the so-called "folded technique" which employs apposition of lipid monolayers over a hole with diameter of 120 μm on a Teflon film [27, 82-84].

For folded bilayers, we pretreated the Teflon film with hexadecane in pentane and then secured the film to a Teflon chamber such that it separated two bath solutions. As electrolyte, we used a buffer containing 150 mM KCl, 10 mM Hepes with pH 7.4, and 1 mM MgCl2. All bilayers used in electrophysiological experiments presented in this thesis were done with a 1:1 w/w mixture of DOPS and DOPE lipids at concentration 20-25 mg/mL in pentane. This phospholipid solution was added to each chamber. We formed the bilayer by raising the buffer in each chamber until the hole on the Teflon film was completely submerged in the electrolyte buffer. Lipid monolayers in each chamber come in contact over the hole to form the lipid bilayer [27, 83].

As an electronic model, the bilayer is represented as a resistor and a capacitor in parallel. By measuring the capacitance and the conductance (inverse of resistance) across the bilayer, we determined whether or not we formed a bilayer. Thus, we raised and lowered the liquid level in each chamber until we measured a conductance of about 1 pS (or greater than 10 GΩ) [83]. Furthermore, the bilayer has a capacitance due to the storage of charge near its surface. The DOPS lipids have a negatively charged head group that attracts the cations in the electrolyte buffer. The capacitance of the bilayer can thus be approximated using the equation for a parallel-plate capacitor given by

$$C = \frac{\epsilon_0 \epsilon_1 A}{d},$$

where C is the capacitance, A is the surface area of the bilayer, d is the bilayer thickness, ϵ_0 is the permittivity of free space, and ϵ_1 is the dielectric constant of the lipid [85]. By applying an en electric field across the bilayer, the capacitance is measured given the relationship

$$Q = CV,$$

where Q is the charge stored and V is the potential difference across the bilayer [85].

2.3 Planar Lipid Bilayer Recordings

We measured current using Ag/AgCl electrode pellets placed in each side of the PLB chamber. Both electrodes are connected to a pre-amplifier, or headstage. One of the electrodes was connected directly to the amplifier (referred to as the “hot wire”), while the other was connected to ground as a reference electrode (see figure 11). Before performing electrical recordings, we verified that the bilayer was stable for several

minutes and that the capacitance of the bilayer was above 70 pF. When both criteria were fulfilled, we then added the peptide to the cis (hot wire) chamber. We added the specific Aβ peptide by direct addition by the addition of specific Aβ proteoliposomes. Aβ concentrations ranged from 0.5 μM to 18 μM. A liposome is an artificially made vesicle composed of a lipid bilayer. A proteoliposome is a liposome into which a protein (or peptide) has been inserted. Adding Aβ to proteoliposomes into the PLB chamber promoted liposome fusion into the lipid bilayer and with it the inserted Aβ peptide. Thus, we increased our probability and likelihood to measure ion channel activity.

While a proteoliposome preparation was important for us to see the channel activity, directly adding peptide to one of the Teflon chambers was just as important. Through direct addition, we could determine whether or not the specific Aβ peptide could bind and insert to the membrane on its own and form channels. There were occasions where direct addition did not show activity after an extended period of time, thus we "refolded" the bilayer to help infuse the peptide into the bilayer. Any channel activity measured after refolding the bilayer was noted and taken into account in our results. This is similar to the proteoliposomes approach in that we aid fusion of the peptide to the bilayer. Whether the specific peptide needs help inserting to the membrane on its own helps us better understand the overall membrane binding mechanism for the Aβ molecule tested. We collected all data using voltage clamp mode (constant voltage). We used a filter-cutoff of 2-3 kHz and a sampling frequency of 15 kHz for all recordings. For representation in figures, we filtered the current traces with a digital Gaussian low-pass filter with a cutoff frequency of 50 unless noted otherwise [27]. We used a custom made

LabVIEW program to acquire data and Clampfit 10.2 to analyze current vs. time traces [27, 83, 84].

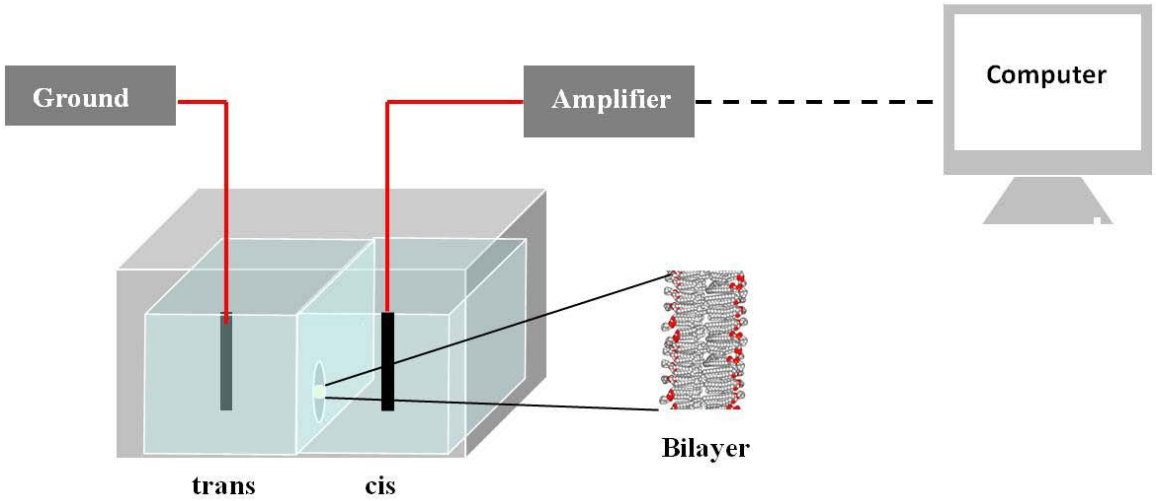

Figure 11: Schematic of a PLB setup for bilayer recordings. It is composed of two chambers separated by a Teflon film with a small hole. When raising the liquid level in each chamber, a lipid bilayer is built on the hole of the Teflon film. We measure the current using electrodes submerged in the solution of each chamber: one is connected to the amplifier and the other is connected to ground as a reference electrode. The recordings are controlled and displayed using a LabVIEW program. This schematic representation of the bilayer setup is a modified version from one originally made by Panchika Prangkio (University of Michigan Ph.D. student).

2.4 Learning the Technique

Learning to perform planar lipid bilayers (PLB) experiments, including making bilayers, preparing lipids and proteins, and analyzing data is time a consuming undertaking. Prior to beginning work with Aβ, I was trained to do PLB's using a peptide known to form well defined, homogeneous current jumps. As a model for training I used gramicidin A (gA). gA exhibits model activity and by intentionally repeating PLB experiments from Capone et al 2007 [84], I established a working knowledge of how to study single ion channel conductance.

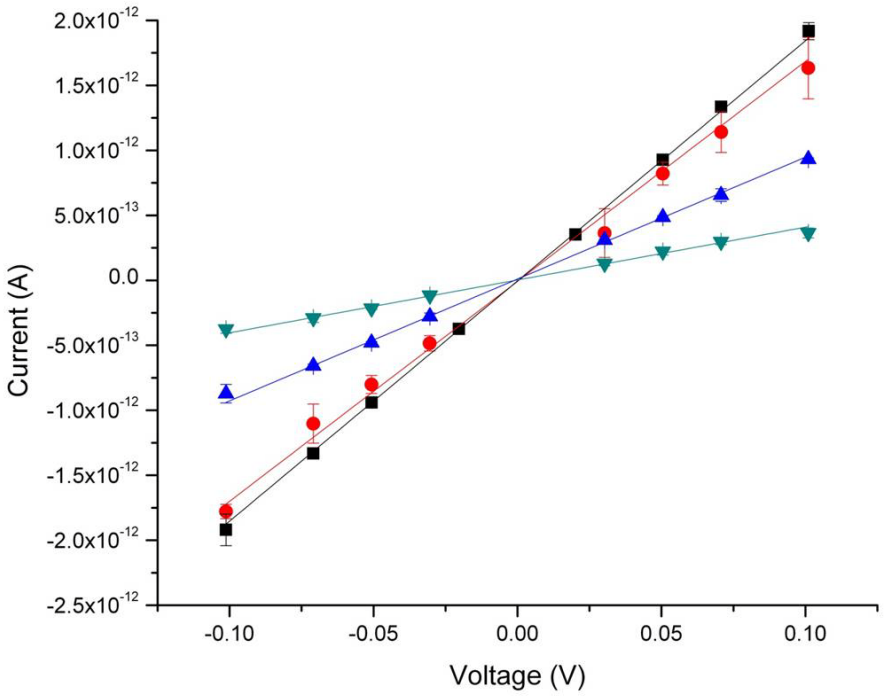

Figure 12: PLB technique training (I). Conductance of gA at different molar concentrations in KCl solution. (■) 1M with 18.5 ± 0.1 pS, (●) 0.5 M KCl with 16.9 ± 0.5 pS, (▲) 0.1 M KCl with 9.38 ± 0.07 pS, (▼) 0.02 M KCl with 4.07 ± 0.12 pS. The values represented here are in agreement with those previously reported [84].

After forming the bilayer and determining its stability (as described above), the first characteristic to note of channel formations was the current-voltage relationship. Within a ±100 mV range, I observed a linear relationship between current and voltage as previously published (see graph depicting behavior-figure 12) [84]. Furthermore, electrolyte concentrations of the buffer used in these PLB experiments had an effect on conductance levels [84]. At higher KCl concentrations, we observed the expected increase in the conductance of measured gA channels. This relationship is depicted in the graph of figure 12, in which each set of data points refers to buffers of different

concentrations. In figure 12, it is clear that higher concentration result in steeper curves (i.e. higher conductance). A typical current versus time trace depicting single channel conductances of gA is presented in figure 13. When a channel opens and conducts cations there is a step in the current activity, indicating ionic current detected by the reference electrode. While recording, we changed the polarity of the voltage to show that these steps were homogeneous.

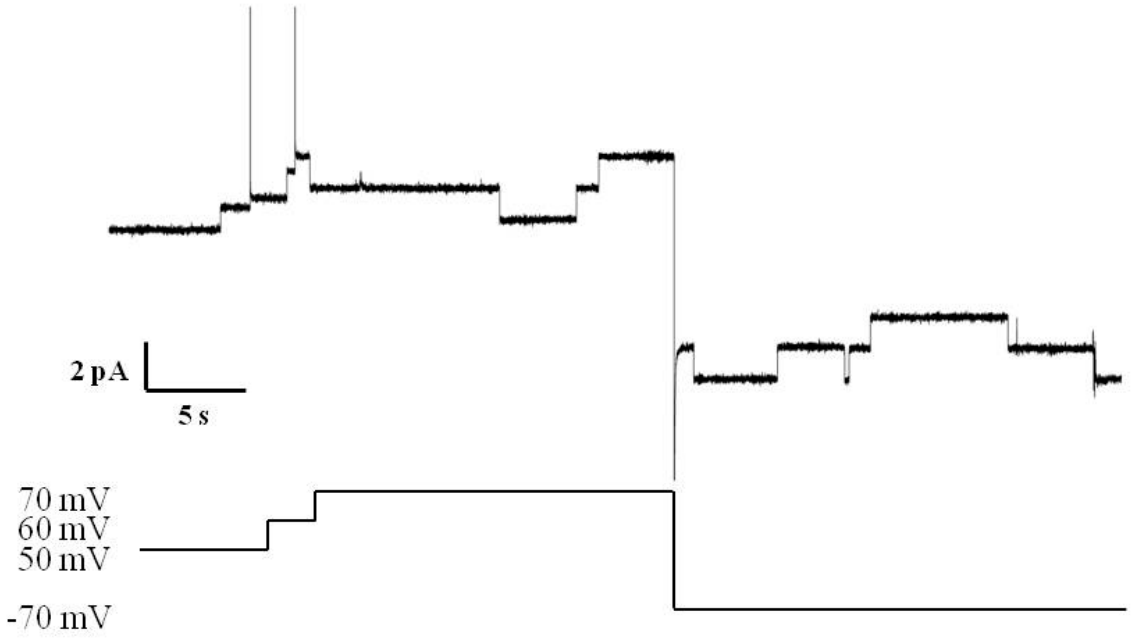

Figure 13: PLB technique training (II). Current vs. time trace of gA in 1 M KCl solution showing homogeneous single ion channel traces of gramicidin A. The step size increases with the applied potential and the current amplitude is dependent on the voltage bias. The bilayer was composed of DiPhyPC lipid.

The goal of repeating these gA experiments was a way to build a firm base in the mechanics of PLB experiments and single ion channel conductances. This objective was accomplished as demonstrated by the gA results summarized in figures 12 and 13. This training was necessary to gain a basic understanding of channel behavior.

Comprehending channel behavior is essential when working with amyloid channels, as these channels typically show heterogeneous conductances and other complex behaviors.

3. RESULTS AND DISCUSSION

3.1 Membrane Durability

Before we began conducting experiments with peptide, we needed a baseline to determine if the lipid combination we used (1:1 w/w DOPS and DOPE) would work and a control from which we could verify inactivity from activity. We chose a DOPS/DOPE lipid composition because Aβ requires a negatively charged membrane. Thus, we performed seven PLB experiments with the folded technique in which no peptide was added. By carrying out "membrane only" experiments, we confirmed a functional system. We allowed these experiments to run for up to 4 hours. We made periodic capacitance measurements monitor membrane quality and stability. We found that in these seven experiments, the average bilayer conductance was 0.86 ± 0.40 pS (n=7). The lowest conductance we obtained was 0.32 pS and the highest was 1.36 pS. These conductances corresponded to membrane resistances in the range of 3125 GΩ and 735 GΩ, respectively. Thus, when verifying the stability of our membranes prior to the addition of the Aβ peptide, we ensured the membranes fell within the range measured in our control experiments. These results show that we could obtain stable anionic membranes for extended periods of time.

To further examine DOPS/DOPE bilayer integrity, at the end of the testing period we added gramicidin A, a peptide known to form well defined ion channels upon addition to both PLB chambers. After 4 hours of recording with DOPS/DOPE bilayers, we added gA and saw gA channel activity, thus demonstrating that DOPS/DOPE bilayers that are stable over time and permeabilizable by gA.

3.2 Aβ42-Wild Type Forms Ion Channels in Lipid Bilayers

Much work has been done and repeated to propose that the amyloid-beta (Aβ) peptide forms ion channels in lipid membranes [13, 22, 27, 40-43, 49, 50, 71, 72, 86]. The "Aβ ion channel hypothesis" suggests that Aβ forms ion channel-like pores in lipid membranes causing transmembrane currents that are typical of Aβ ion channels [13, 22, 27, 40-43, 49, 50, 71, 72, 86]. Upon adding Aβ peptide to one side of the PLB chamber, Aβ must first bind to the bilayer and make a conformational change to allow the Aβ peptide to insert into the bilayer. Once in the bilayer, monomers or oligomers must interact with one another to form a pore-like structure. There are three different types of ion channel activity that have been described for Aβ channels [86]. The first type of channel activity is the "bursting" fast cation channel which, as its name implies, is a short burst of activity that gives a nonlinear current-voltage relationship [86]. The second type of channel activity is the "spiky" fast cation channel which is similar to a burst of activity; however, the spike is more short-lived when compared to bursting activity [86]. Lastly, the third type of channel activity is the "step" or "step-like" activity [86]. With the step-like behavior a clear, defined jump in current is seen as a channel opens and closes.

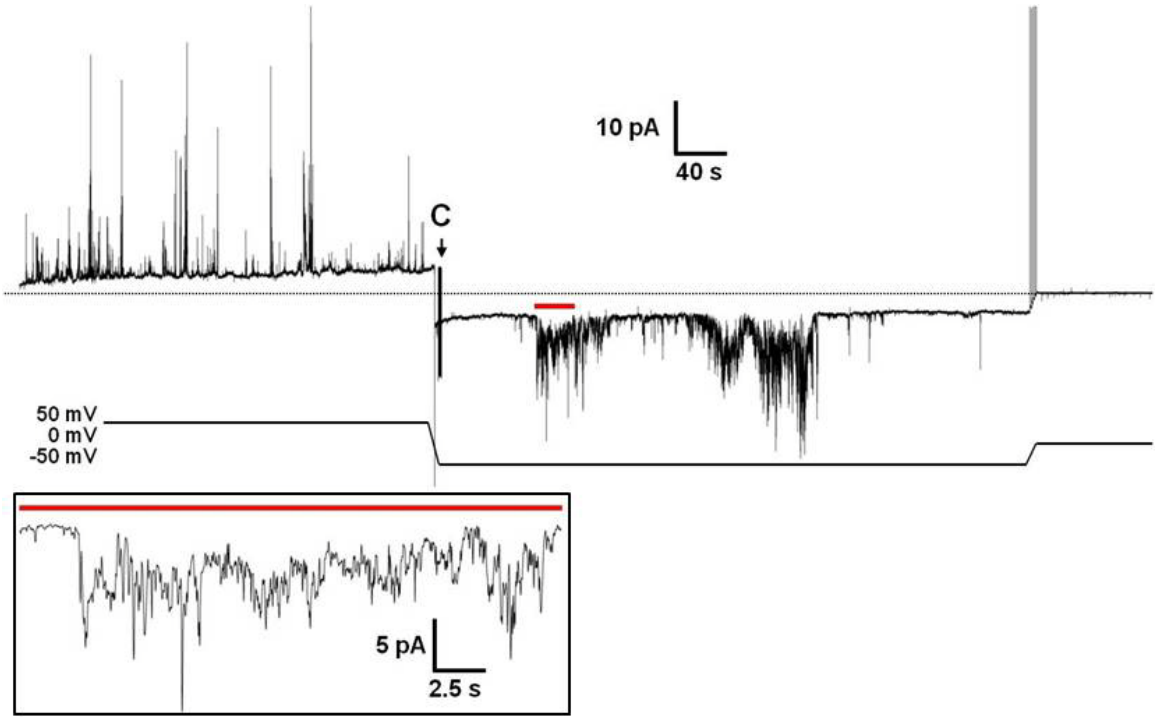

Figure 14: Current vs. time trace of channel activity of Aβ42-WT. The channel activity shown here depicts spikes and bursts typical of Aβ42-WT in folded bilayers. The voltage vs. time trace shown below follows the changes in applied potential to the current vs. time trace above. The inset indicated by the red bar shows bursting activity at a higher time resolution. The vertical line marked with letter C indicates a capacitance measurement during the recording. Aqueous solution used contained 150 mM KCl, 10 mM Hepes pH 7.4, and 1 mM $MgCl_2$. The bilayer was composed of 1:1 w/w DOPS:DOPE.

The different types of current activity from Aβ42 wild type (Aβ42-WT) in a DOPS/DOPE lipid bilayer are illustrated in the current versus time trace displayed in figure 14. Figure 14 illustrates bursting, spiky behavior of Aβ42-WT channels with 50 mV of applied voltage. We then changed the polarity of the voltage to -50 mV, measured capacitance and, as shown in figure 14, the channel began to exhibit a bursting fast cation channel. Finally, we set the voltage to 0 mV and the channel activity subsided, showing that the channels for Aβ42-WT are voltage independent. The inset of figure 14 is a close up of the bursting activity, depicting the representative behaviors of Aβ42-WT channel activity. The only truly apparent difference between bursting and spiky behavior is that

the bursting channel activity is characterized by the absence of the long closures of channels [86]. Figure 15 reiterates the spiky, bursting nature shown in figure 14; however, figure 15 better depicts the current-voltage relationship for Aβ42-WT channels. As we decreased the voltage from -80 mv to -50 mV in 10 mV steps, the conductance level decreased as well. The inset of figure 15 shows a higher time resolution of the step-like activity seen with Aβ42 channels. These steps are less frequent in folded bilayers than they are in painted bilayers.

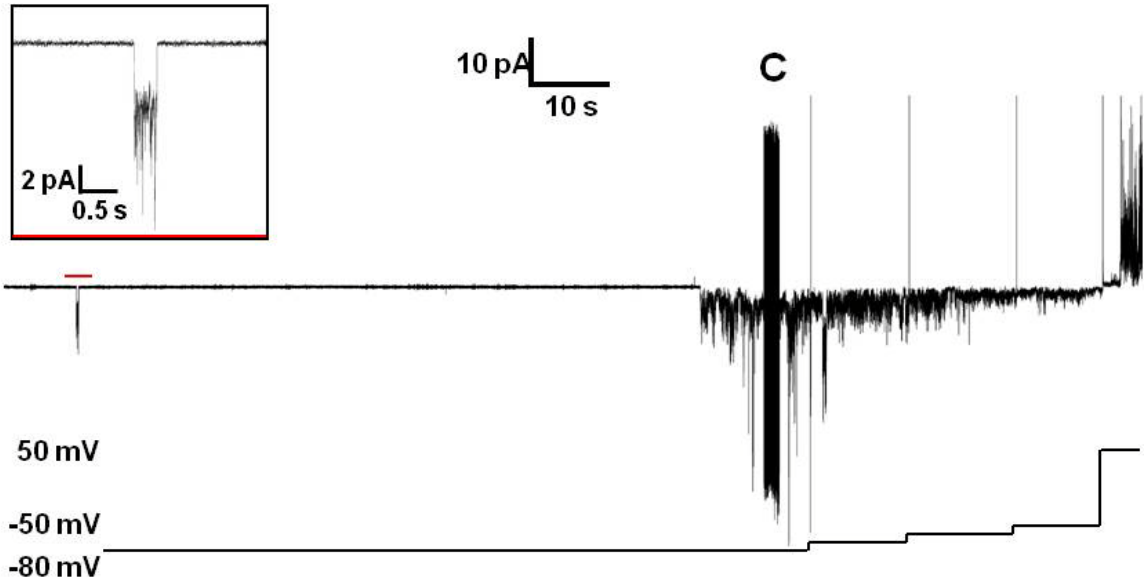

Figure 15: Aβ42-WT types of channel activity. Current vs. time trace illustrating all types of activity of Aβ42: spikes, bursts, and steps. The activity shown occurred 1 hour after refolding the bilayer. Below the current trace, the applied voltage indicates when we decreased the voltage, resulting in decreased conductance. We changed the polarity from negative to positive and the current amplitude follows, indicating a linear I-V respone. The inset of the figure displays a higher time resolution of the current vs. time trace highlighting a single step with an average conductance of 80 pS. The vertical line marked with letter C indicates a capacitance measurement during the recording. Aqueous solution used contained 150 mM KCl, 10 mM Hepes pH 7.4, and 1 mM $MgCl_2$. The bilayer was composed of 1:1 w/w DOPS:DOPE.

Figure 16 A-C depicts 45 minutes of recording and the ability of zinc to block a portion Aβ42-WT activity as previously shown [22, 40-43, 49, 71]. The arrow in figure

16 A points to the time at which zinc was added to the same chamber as Aβ42-WT. The channels are not immediately blocked by zinc (figure 16A), yet, as the experiment progressed we observed decreased conductances (figure 16 B). A change in polarity (figure 16 C) appeared to induce a temporary increase in conductance. This resurgence in activity is blocked by zinc and remains mostly inhibited for final duration of the experiment (figure 16 C).

Figures 14, 15, and 16 show ionic current with multiple conductance levels and this heterogeneous nature is typical of Aβ ion channels and other channel forming amyloids. One possible explanation for this behavior is that the channels consist of distinct oligomeric species, forming distinct channel structures [13]. Given the different conductances of the Aβ channels, this could explain the variance in conductance measured in the electrical recordings. In 13 experiments with Aβ42-WT we measured channel activity in 6 cases, making the frequency of channel activity 46% which is comparable to reports from previous work with Aβ42 [48, 49]. Interestingly, we also found that different lots of Aβ42 had an effect on the percentage of channel activity observed. This suggests that the aggregated state of Aβ42 effects channel activity, reaffirming the notion that the aggregation state influences Aβ42's ability to permeabalize the membrane. Our results show that activity occurred at concentrations as low as 0.5-1 μM. We did not exceed concentrations of 4.5 μM. Channel-like behavior was never observed in bilayers without the addition of the peptide, as shown by the membrane only experiments described above.

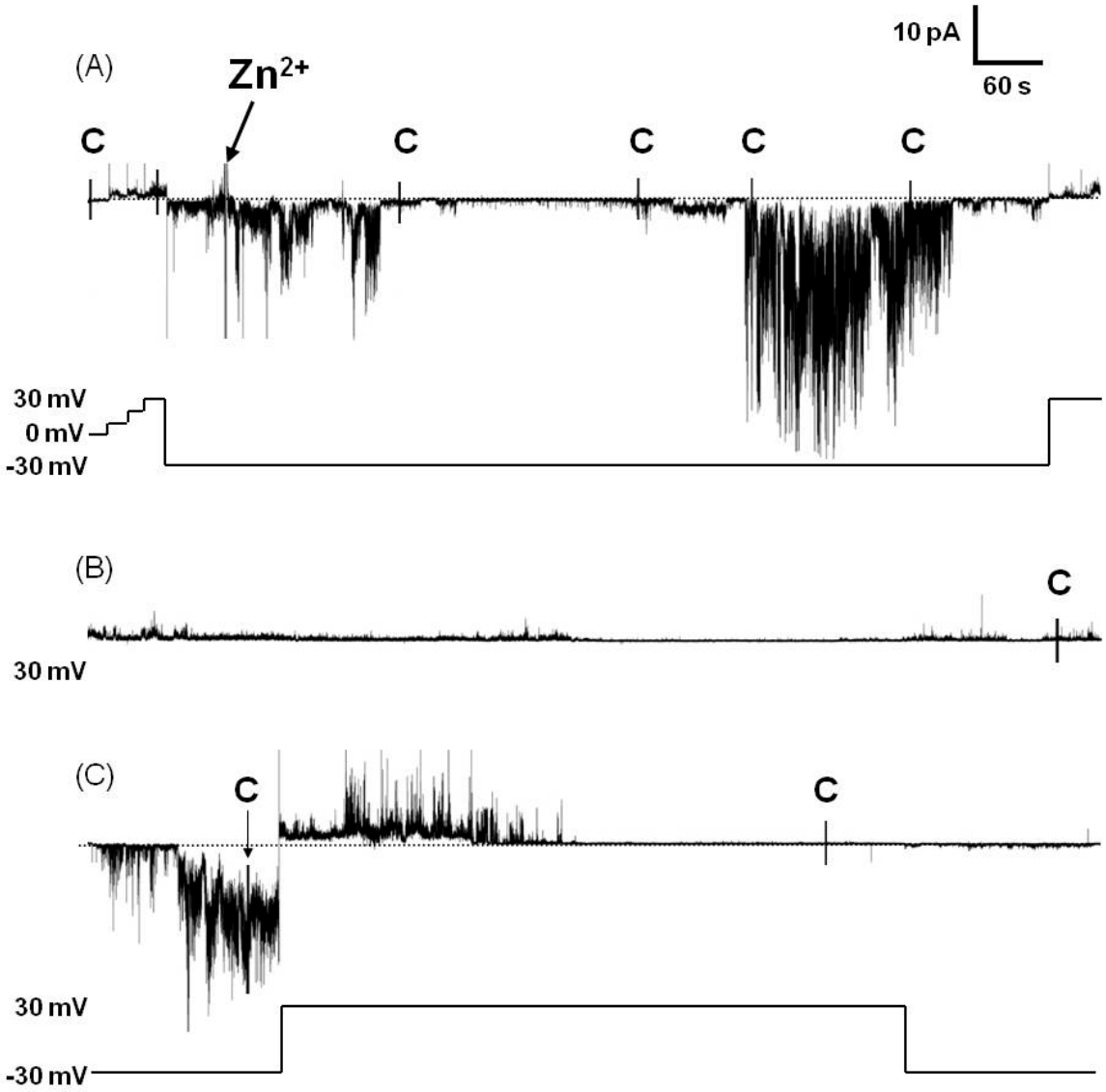

Figure 16: Aβ42-WT is inhibited by Zn^{2+}. Three continuous current vs. time traces totaling 45 min of recording with 4.5 μM of Aβ42-WT. The bilayer shown was refolded and continued from the same experiment conducted in figure 15. (A) We added Zn^{2+} to final concentration of 2 mM and stirred. The activity was not immediately inhibited and decreased gradually as shown in panels B and C. (B) We maintained the voltage bias to 30 mV. (C) Changing the polarity of the applied potential seemed to temporarily induce an increase in conductance. We stirred again and the activity was blocked and remained mostly inhibited for the remaining 12 minutes of the experiment. The vertical lines marked with letter C in all panels indicate a capacitance measurement during the recording. Electrolyte solution used contained 150 mM KCl, 10 mM Hepes pH 7.4, and 1 mM $MgCl_2$. The bilayer was composed of 1:1 w/w DOPS:DOPE.

Although work showing channel activity of Aβ42-WT has previously been done [42, 45, 48, 49], one prerequisite for this work was to characterize Aβ42 activity in our

membrane/buffer system. We also needed a reference from which we could compare our results with the Aβ42 mutants. To our knowledge this is the second report showing Aβ activitt with folded bilayers [27]. Other groups studying Aβ ion channel formations in model membranes used painted bilayers [41-43, 48, 49, 86]. Generally, folded bilayers are considered to be a better model of bilayers because of they contain a lower level of solvents in the bilayer. We found that activity of Aβ42 in folded bilayers generally exhibited more spiky and bursting activity than step-like activity.

The combined results of membrane only experiments and Aβ42 activity in DOPS/DOPE folded bilayers validate a system to test the activity of Aβ42 mutants. In order to gather structural information of Aβ ion channels, we studied amino acid substitutions of Aβ42. By studying these mutants, we intend to infer structural features of Aβ and its function in membranes. This *functional* approach provides structural information presently not capable by other techniques.

3.3 Aβ42-F19P Does Not Exhibit Ion Channel Activity

The amino acid proline is under-represented in β sheets of proteins of known structure [53]. Thermodynamic studies of amino acid replacements in model proteins place proline as being one of the amino acids least compatible with β sheet structure [52, 53, 87-89]. Consequently, proline mutagenesis on Aβ has been intensively studied, specifically the ability of these types of mutants to form fibrils [52, 53, 87-89]. Proline is energetically unfavorable in the extended cross-beta sheet structure [88] and, as a result, prohibits amyloid aggregation [52, 53, 87-89]. A common proline mutant in these works the replacement of phenylalanine, F, with proline, P, in the nineteenth position (Aβ42-

F19P). The substitution with proline introduces a “kink” in the U-turn strands of the peptide.

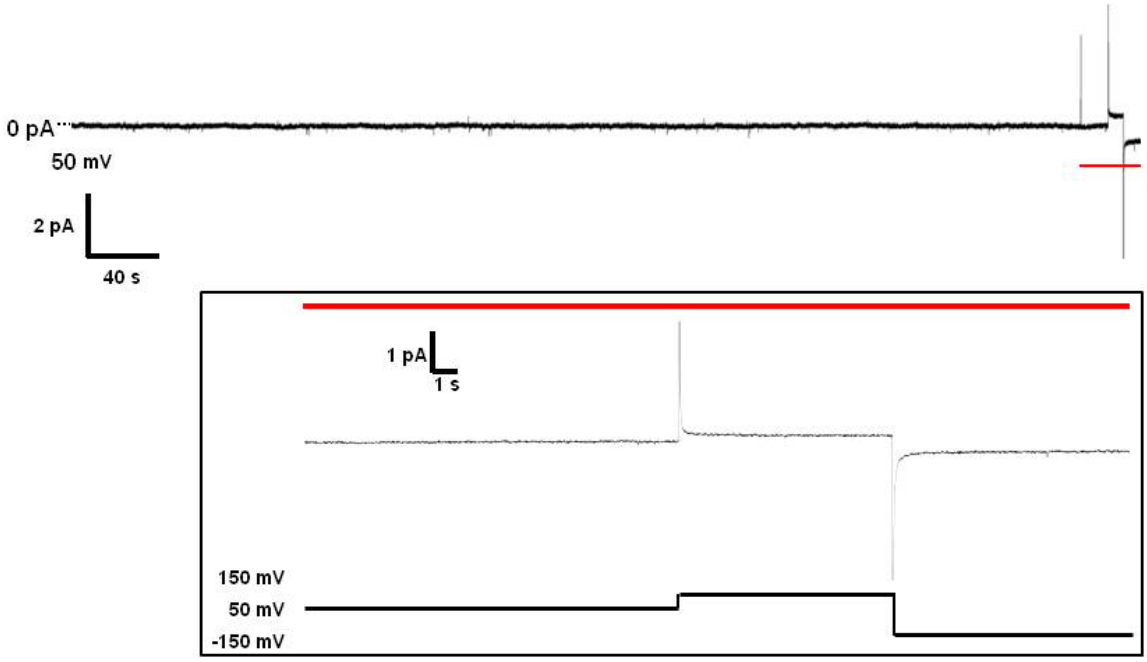

Figure 17: Representative current vs. time trace of Aβ42-F19P. The trace shows F19P at 4.5 μM with no activity. The inset shows the lack of activity for applied voltages as high as ± 150 mV. These 4 hour bilayer experiments were repeated 10 times with no channel-like activity observed. Aqueous solution used contained 150 mM KCl, 10 mM Hepes pH 7.4, and 1 mM $MgCl_2$. The bilayer was composed of 1:1 w/w DOPS:DOPE.

Jang et al 2010 predicted and showed that the fragment Aβ17-42 with the F19P substitution exhibited no channel activity [13]. We show here (figure 17) that Aβ42-F19P exhibits no channel activity, suggesting that the proline substitution in this position hinders the Aβ conducting structure. Figure 17 shows a current versus time trace of the nonconductive Aβ42-F19P mutant. At voltages as high as ±150 mV, there was still no visible conductance from channel formations (inset of figure 17). In more than 40 hours of recording for Aβ42-F19P, we observed *only* 100 seconds of very channel activity. All

of this activity is presented in figure 18. The channels displayed in figure 18 have conductances of 4.6 pS and 2.2 pS (below the level for gA in this membrane/electrolyte system), compared to the wide range of higher conductances for Aβ42-WT, generally between 50 pS and 1 nS (see figures 14-15).

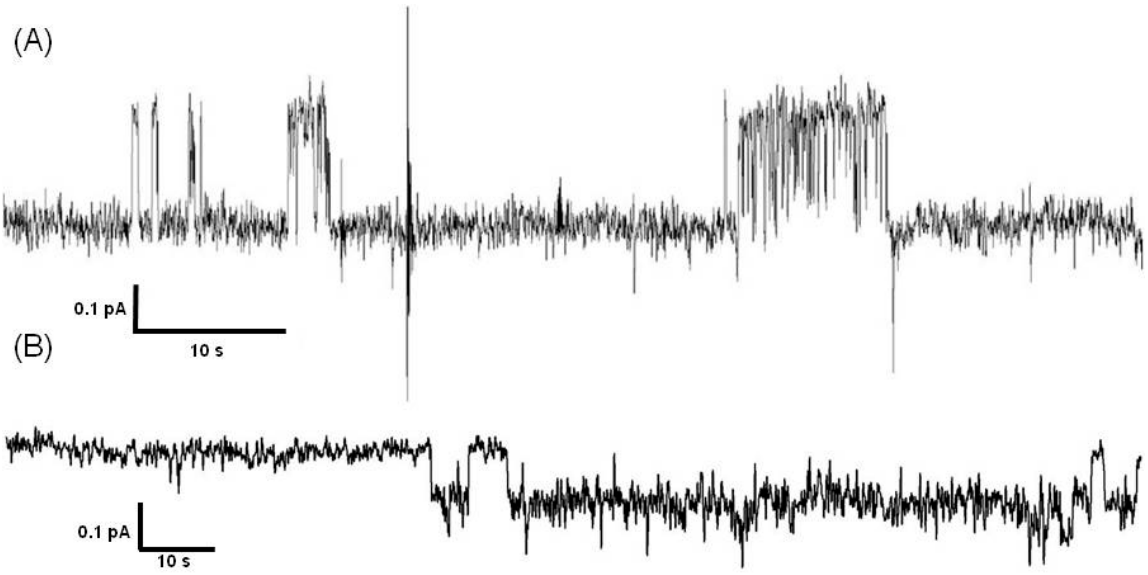

Figure 18: Aβ42-F19P may form collapsed channels. Current vs. time trace showing low conductance, step-like activity for Aβ42-F19P at 4.5 μM. (A) The calculated conductance for all steps shown was (A) 4.6 pS at an applied voltage of 50 mV and (B) 2.2 pS at an applied voltage of -50 mV. This is the only activity observed in over 40 hours of recording. Aqueous solution used contained 150 mM KCl, 10 mM Hepes pH 7.4, and 1 mM $MgCl_2$. The bilayer was composed of 1:1 w/w DOPS:DOPE. These traces were filtered at 10 Hz and could not be seen otherwise.

These low and unique conductance measurements in over 40 hours of recording might suggest that Aβ42-F19P forms collapsed pores on the bilayer. This hypothesis is currently being tested by AFM imaging and was also made and tested for the p3-F19P [13, 14]. The results presented here suggest a similar conclusion for the full length Aβ peptide. Aβ42-F19P was tested in both painted (n =7) and folded (n =10) bilayers at concentrations ranging from 4.5-13.5 μM. We did not test the effect of zinc with Aβ42-F19P as there were essentially no conducting ion channels recorded. We verified bilayer

integrity at the end of the 4 hour F19P experiments by adding gA and observing its channel formations. Preliminary AFM images of Aβ42-F19P reconstituted in lipid bilayers further suggest the formation of collapsed pores (data not shown). At higher magnification, we saw central pore-like features. The annular structures look similar to those previously described for Aβ40 and Aβ42 channels [15-17, 19-22]. These preliminary AFM images of Aβ42-F19P mutant were done by Laura Connelly, a fellow graduate student in Prof. Ratnesh Lal's laboratory.

Molecular dynamics (MD) simulations of the Aβ42-F19P mutation are currently in progress, and we predict that the simulations of the proline substitution will show obstruction of the ion flux across the pore, as shown for the p3-F19P peptide [13].

3.4 The Aβ42 Cysteine Mutations

The following mutants are the first in a series in which a single amino acid is substituted with a cysteine residue in Aβ42. Cysteine has a sulfhydryl group that is reactive. The intended objective for all of the cysteine mutations is to take advantage of cysteine's sulfhydryl group by reacting it with MTS reagents; the goal being to test in membrane if the Aβ mutated residue is in or near the mouth of the pore and, hence, exposed to the solution. Obtaining such information we can help elucidate the channel structure of Aβ42 in bilayers. Our long term aim is to determine the pore structure of the N and C termini, as well as the structural core. We chose cysteine mutations Aβ42-D1C, Aβ42-A42C, and Aβ42-F20C.

Before performing experiments involving the cysteine-MTS reagent reactions, we needed to determine if these mutants could form channels and whether the channel

activity could be sustained. Moreover, we needed to analyze how closely the channel activity of these cysteine mutations mimicked the Aβ42 wild type; i.e. we needed to validate: types of activity, how often activity occurs, whether or not activity is sustained, and whether or not zinc blocks channel formations.

3.4.1 Aβ42-F20C Forms Ion Channels

For this mutant, phenylalanine was replaced with cysteine in the twentieth position (Aβ42-F20C). To our knowledge, ion channel activity for the F20C mutant has not previously been studied; therefore, the type of activity (inactive, steps, spikes, or bursts) expected was based on hypotheses. We found that the Aβ42-F20C mutant has the ability to form ion channels. We performed 7 experiments with Aβ42-F20C addition of which 4 exhibited activity (or in 57% of cases). In all experiments, we added Aβ42-F20C by direct addition. We initially added the peptide to a final concentration of 4.5 μM and then added 4.5 μM every 45 minutes until a final concentration of 13.5 μM was reached. Under these conditions, Aβ42-F20C activity appears mostly as spikes and bursts and occasionally as short-lived step-like activity. Figure 19 shows the spiky and bursting activity of Aβ42-F20C. We also found that Aβ42-F20C channel formations could be blocked by the addition of zinc (see figure 20).

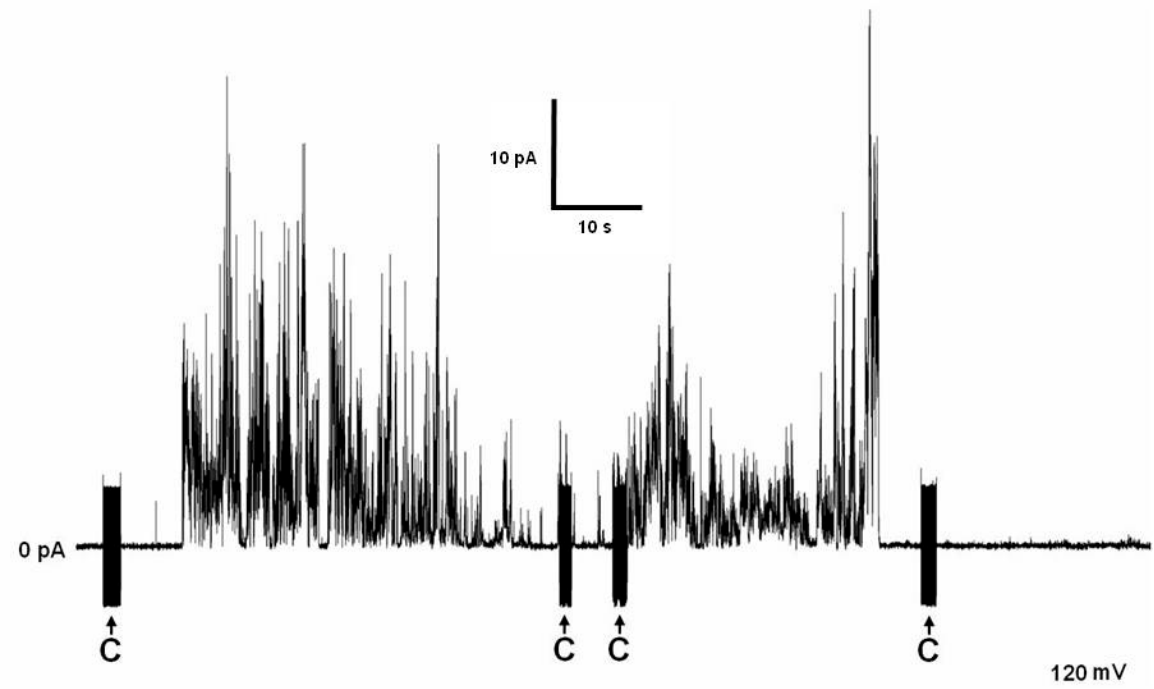

Figure 19: Current vs. time trace of channel activity by the Aβ42-F20C mutant. Channels formed by Aβ42-F20C mostly exhibited spiky, bursting activity with conductance as high as 420 pS; however, there are well defined channel openings and closings noticeable among the bursts. The vertical lines marked with letter C indicate a capacitance measurement during the recording. Electrolyte solution used contained 150 mM KCl, 10 mM Hepes pH 7.4, and 1 mM $MgCl_2$. The bilayer was composed of 1:1 w/w DOPS:DOPE.

Figure 20 A shows a current trace of 15 minutes in which the voltage at the start is -50 mV and active channels are present. We then lower the voltage back to the baseline current to determine the reversal potential. The reversal potential indicates the point at which the activity shifts from negatively biased current activity to positively biased current activity. We found the reversal potential to be about -1.5 mV (figure 20A).

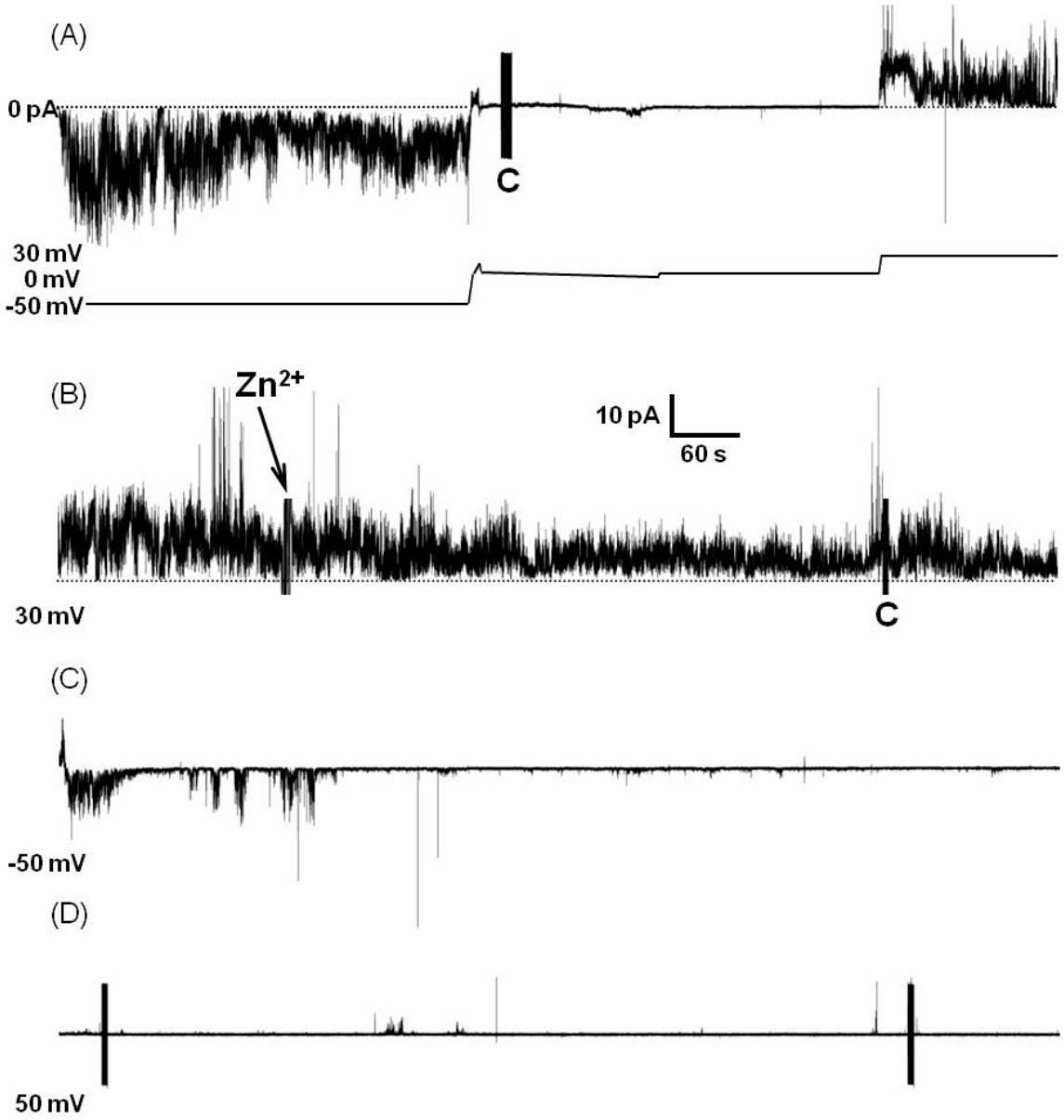

Figure 20: Aβ42-F20C is inhibited by Zn^{2+} ions. Four continuous current vs. time traces totaling one hour of recording with 9 μM of Aβ42-F20C. (A) We found channel activity of Aβ42-F20C to show large sustained bursts and spikes with fast openings and closings. Below this current trace, we show the applied voltage used to estimate the reversal potential (-1.5 mV). (B) We added Zn^{2+} to a final concentration of 0.5 mM and stirred. The activity was not immediately inhibited and decreased gradually as shown in panels C and D. (C) We changed the voltage bias to -50 mV. (D) After 15 minutes, we changed the applied potential to 50 mV. At this point the channel activity is mostly inhibited with occasional events. The vertical lines marked with letter C in panels A, B, and D indicate a capacitance measurement during the recording. Aqueous solution used contained 150 mM KCl, 10 mM Hepes pH 7.4, and 1 mM $MgCl_2$. The bilayer was composed of 1:1 w/w DOPS:DOPE.

Subsequently, we increased the voltage to 35 mV and the activity is still present. Figure 20 B is a continuation of the trace in figure 20 A, also 15 minutes in length. In figure 20 B, Zn^{2+} is added within the first 3 minutes to the same side to which Aβ42-F20C was added with a final concentration of 0.5 mM. After the addition of Zn^{2+}, the activity begins to subside, although not immediately. The next 15 minute current trace (figure 20 C) shows that the channels are inhibited by Zn^{2+}. The conductances at the beginning of the current trace in figure 20 D are weaker than those in figures 20 B-C and, ultimately, the Aβ42-F20C channel activity is inhibited by Zn^{2+}. This result demonstrates that the activity of Aβ42-F20C is sensitive to Zn^{2+} ions.

In most hydrophobicity scales, phenylalanine is more hydrophobic than cysteine. This might suggest why Aβ42-F20C exhibits activity with lower amplitude than the wild type peptide. Our results show that the replacement of phenylalanine with cysteine in Aβ42 does not preclude channel formation. This region of the Aβ peptide is central to its ability to form fibrils. The Aβ42-F20C mutant is known to form fibers [69] which suggests that prior to fibril formation, Aβ42-F20C forms oligomers and protofibrils. In fact, scanning cysteine mutagenesis of Aβ40 found that the F20C mutant was accessible to alkylation in the fibril state indicating that F20 is solvent exposed in fibers [69]. The Wetzel group found that the Aβ40-F20C mutant exhibited fibril kinetics similar to the wild type [69]. This might point some similarities between Aβ pores and fiber structures. Aβ42-F20C exhibited activity somewhat mimicking that of the wild type. In future experiments, we would like to test if this residue, as we expect, is exposed on the pore side of the Aβ channel structure.

3.4.2 Ion Channel Formations of Aβ42-A42C Mutant

Alanine was replaced with cysteine in the forty second position of the full length Aβ42 peptide (Aβ42-A42C). Like the Aβ42-F20C mutant, to our knowledge, ion channel activity for the Aβ42-A42C substitution has not been previously studied. We found that Aβ42-A42C has the ability to form ion channels, although its activity is less sustained and frequent when compared to Aβ42 wild type. A42C activity is mostly spiky and bursting as shown in figure 21. The inset of figure 21 shows a higher time resolution of the underlined portion to better represent the described spiky and bursting channel activity. Out of eleven experiments with Aβ42-A42C, seven exhibited activity (63%); however, the activity was of generally lower amplitude and very short-lived. We considered whether the activity of could Aβ42-A42C be enhanced by pre-loading it into liposomes; the idea being to reduce the energetic barrier of peptide insertion into the PLB bilayer.

We used the Aβ42-A42C proteoliposomes preparation in 4 of the 11 experiments and found activity in 3 of these experiments. When using proteoliposomes, the final peptide concentration when added to one side of the PLB chamber was between 0.5-1 μM. In all other experiments Aβ42-A42C was directly added to one side of the PLB chamber. In the direct addition experiments, the final peptide concentration in solution was 3.4-4.5 μM and channel activity was seen in 4 out of 7 cases. Of these 4 cases, channel activity was seen after refolding the bilayer in 3 experiments (for details see materials and methods). We obtained channel activity by “pure” direct addition only in one case out of seven experiments in which activity was detected. Given that 75% of experiments with the proteoliposomes preparation showed activity, as well as activity in

all refolded bilayers, suggests that Aβ42-A42C needs to be aided for membrane insertion. In other words, the A42 residue appears to be involved in the insertion of Aβ42 into the bilayer. Aiding Aβ42-A42C bilayer insertion restores partial activity.

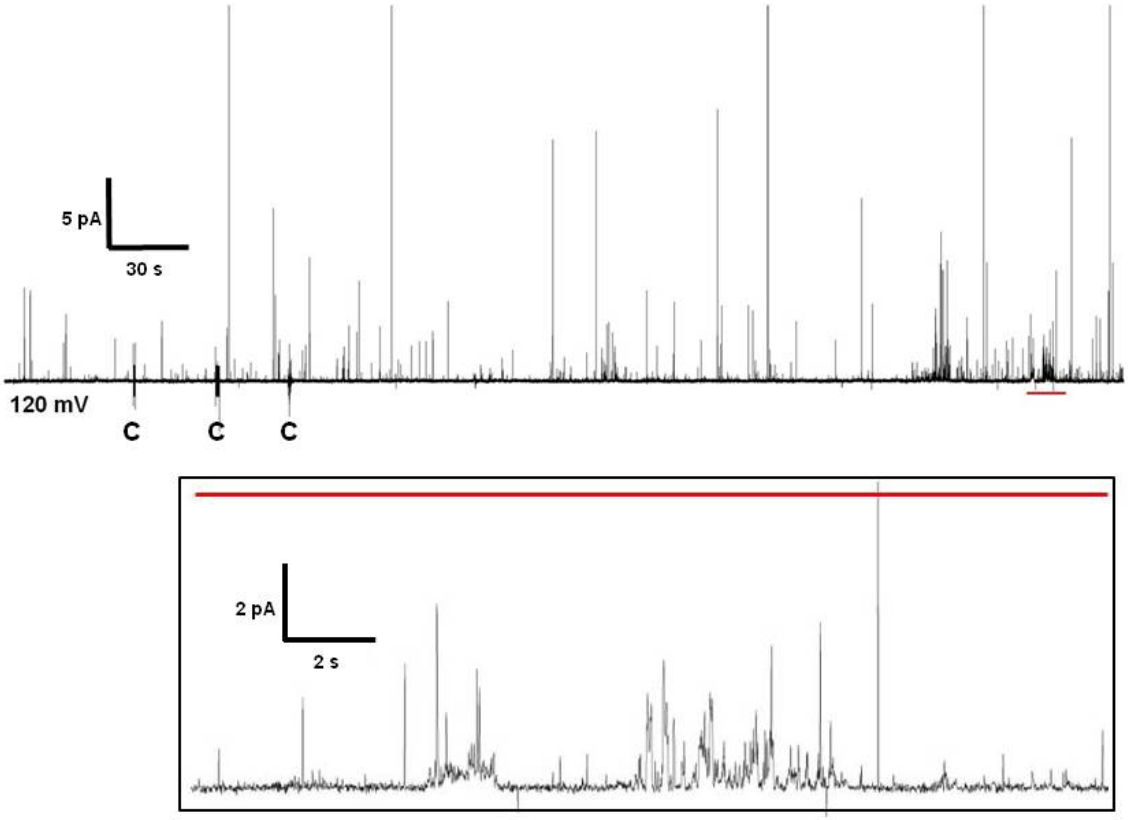

Figure 21: Current vs time trace showing channel activity by the Aβ42-A42C mutant. Channels formed by Aβ42-A42C mostly exhibited spiky, bursting activity with low conductances. Occasionally high amplitude spikes showed conductances as high as 1.1 nS. The inset here shows a higher time resolution, clearly depicting the spiky and bursting nature of the activity typical of Aβ42-A42C. While the activity is more short-lived than Aβ42 wild type, the high conductance level of Aβ42-A42C is still comparable to that of the wild type. The vertical lines marked with letter C indicate a capacitance measurement during the recording. Aqueous solution used contained 150 mM KCl, 10 mM Hepes pH 7.4, and 1 mM $MgCl_2$. The bilayer was composed of 1:1 w/w DOPS:DOPE.

Due to the fact that activity was rarely sustained, we only attempted to block channel activity with zinc in 1 out of 11 experiments. In this experiment, channel activity was only partially inhibited. Alanine is more hydrophobic than cysteine suggesting that in

Aβ channel structures, A42 is buried in the hydrophobic core of the bilayer. Lowering the hydrophobicity of this residue hinders Aβ42 channel formation. Even after aiding insertion of Aβ42-A42C by means of proteoliposomes fusion or refolding the bilayer, we observe mostly spiky, bursting activity that is poorly sustained. These results support the proposed notion that Aβ42 channels have residue A42 buried in the hydrocarbon part of the bilayer. Unlike fibrils where the Wetzel group found that cysteine mutations in the C terminus of the Aβ40 peptide were accessible to alkylation in the fibril state and did not greatly impact fibril stability [69]. In residual samples of Aβ42-A42C we were able to see the formation of visible aggregates. Our findings might point to the C terminus playing an important role in Aβ membrane insertion and channel formation.

Additionally, there are known conformational polymorphisms in this area of the peptide. The Aβ channel structures proposed by Strodel et al 2010 [77] might suggest why we saw diminished channel activity. This model proposed an additional U-turn existing between residues M35 and A42, and if correct, the lower hydrophobicity of cysteine might point to why we obtained lower, poorly sustained conductance levels for Aβ42-A42C [77]. Probing other residues in or near A42 might help determine which conformation is predominant for Aβ42 near the C terminus. Finally, it is clear that the last two additional amino acids of Aβ42 have tremendous effects on many biophysical parameters and exert a difference in the membrane behavior between Aβ40 and Aβ42.

3.4.3 Aβ42-D1C Mutant Exhibits Little to No Ion Channel Activity

For this mutant, aspartic acid, D, was replaced by cysteine, C, into the first position (Aβ42-D1C). We found that the Aβ42-D1C mutant has great difficulty forming

ion channels. In a total of 15 experiments (with proteoliposomes prep and by direct addition), we saw activity in only 3 experiments. For experiments conducted with the proteoliposomes prep, concentrations were about 1 μM, while experiments conducted with direct peptide addition concentrations ranged from 2.3 to 9 μM. Figure 22 shows the predominant lack of activity by Aβ42-D1C in two current traces with constant voltages at both 80 mV and -80 mV of applied potential. The noise at the beginning of both traces is due to stirring in the PLB chamber where we added Aβ42-D1C. The inactivity following the noise from mixing seen in both traces from figure 22 occurred in 12 out of 15 experiments, each lasting about 2 hours in length.

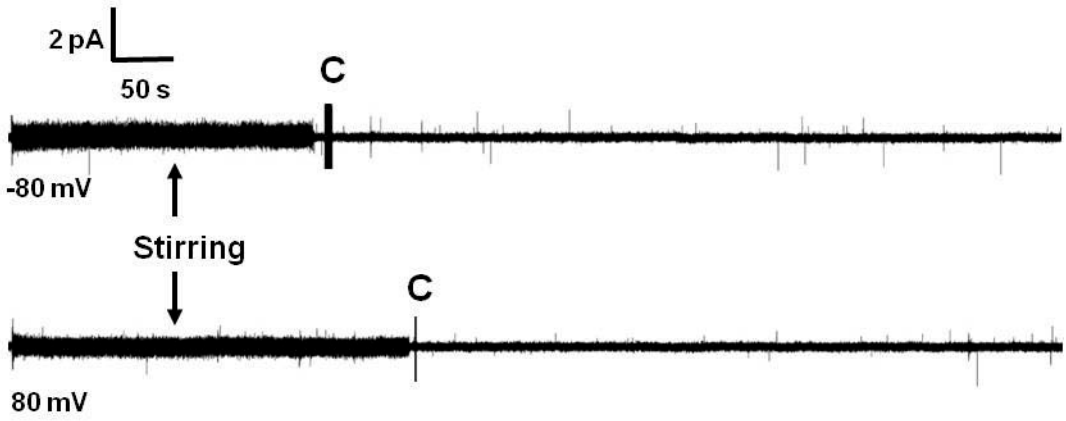

Figure 22: Aβ42-D1C showed a high percentage of inactivity. Two continuous 15 minute current vs. time traces recorded in the same experiment represent the inactivity measured in 12 out of 15 experiments with Aβ42-D1C. The vertical lines marked with letter C indicate a capacitance measurement during the recording. Electrolyte solution used contained 150 mM KCl, 10 mM Hepes pH 7.4, and 1 mM $MgCl_2$. The bilayer was composed of 1:1 w/w DOPS:DOPE

While we found such a high percentage of inactivity, 3 experiments did exhibit channel activity as shown in the current traces of figure 23. Figures 23 A and 23 B are current traces for 2 separate experiments for which we observed minor channel activity,

however, the activity is very short-lived. Figure 23 A shows step-like activity with conductances of 9.7 pS, 3.3 pS, and 2.4 pS with respect to the first, second, and third steps (averaging 5.1 pS). Figure 23 B illustrates spikes and a burst measured in a separate experiment. Both figures are indicative of Aβ42-D1C channel activity; however, the current traces in figure 23 show the entirety of the *only* detected activity throughout those two experiments.

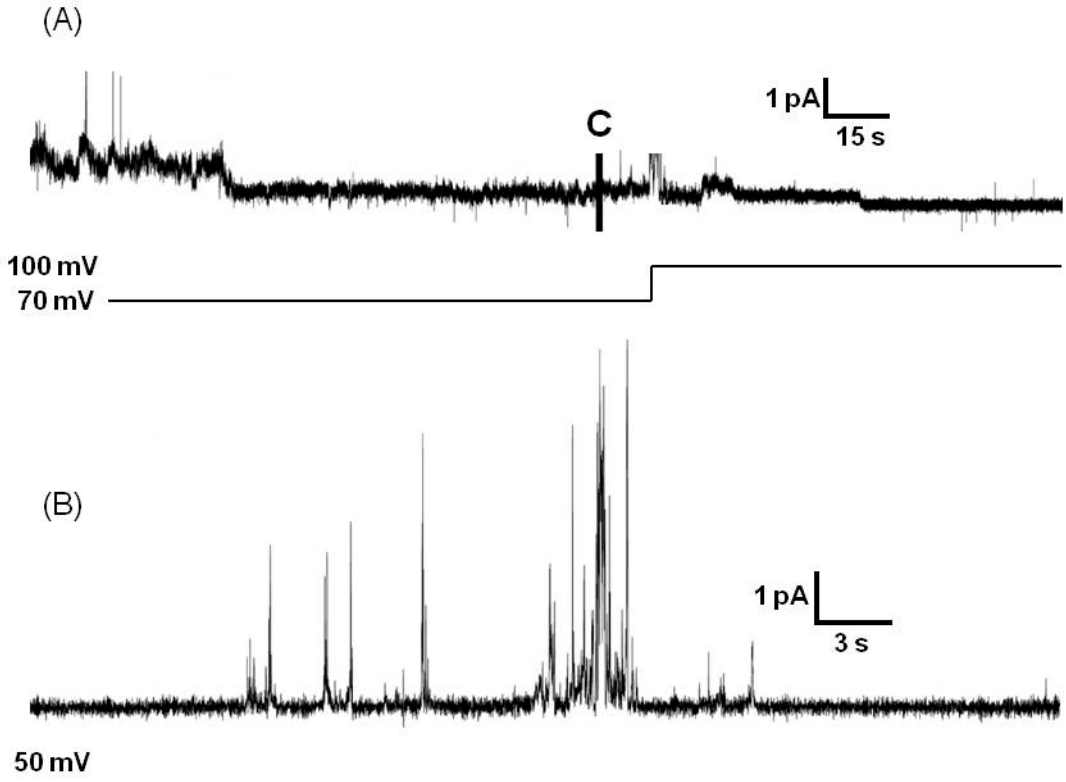

Figure 23: Aβ42-D1C activity is rare in folded bilayers. Two separate experiments with Aβ42-D1C showed low amplitude channel activity, all of which is shown here. (A) We measured the conductance of each step to be 9.7 pS, 3.3 pS, and 2.4 pS, respectively, for an average conductance of 5.1 pS. We did not measure any other channel activity for this experiment. Applied voltage vs. time trace shown below current vs. time trace. (B) The only activity seen in this experiment was spikes and burst shown here. Note that in both current vs. time traces, the activity is short-lived, yet representative of the types of activity seen with Aβ42-WT. The vertical line marked with letter C in panel A indicates a capacitance measurement during the recording. Aqueous solution used contained 150 mM KCl, 10 mM Hepes pH 7.4, and 1 mM $MgCl_2$. The bilayer was composed of 1:1 w/w DOPS:DOPE.

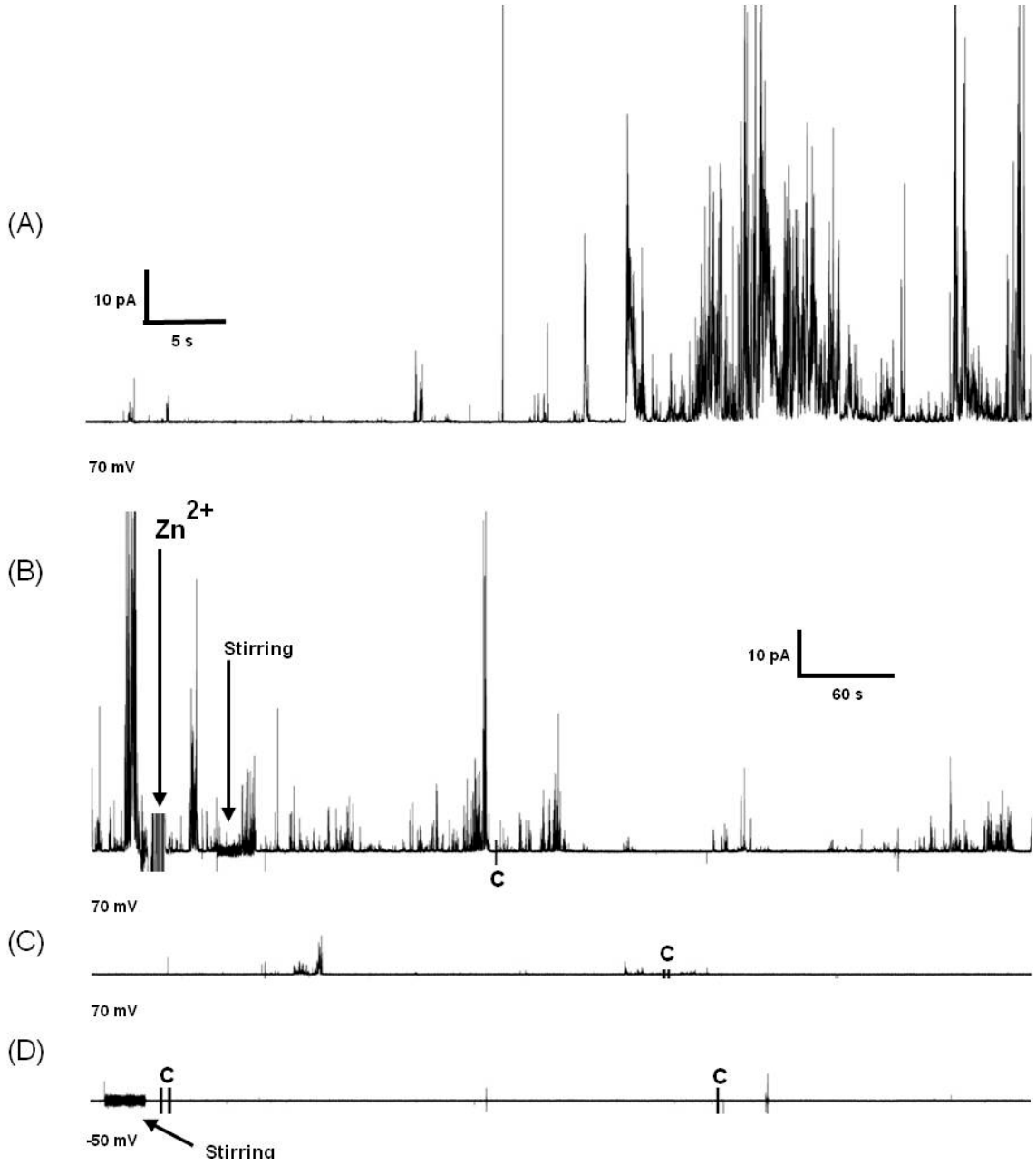

Figure 24: Aβ42-D1C is inhibited by Zn^{2+}. Four continuous current vs. time traces totaling 31 min of Aβ42-D1C at 2.3 μM. (A) The activity is in the form of spikes and large bursts much like Aβ42-WT and was obtained after refolding the bilayer. (B) We added Zn^{2+} to a final concentration of 0.5 mM and stirred. (C) In the following 10 minute trace, channel activity is mostly inhibited and in (D) the last 10 min of recording there are no spikes or bursts, suggesting Zn^{2+} inhibition. The vertical lines marked with letter C indicate a capacitance measurement during the recording. Electrolyte solution used contained 150 mM KCl, 10 mM Hepes pH 7.4, and 1 mM $MgCl_2$. The bilayer was composed of 1:1 w/w DOPS:DOPE.

In one case of out fifteen, we did see sustained activity with Aβ42-D1C. We inhibited this activity with zinc (figure 24). Figure 24 A shows the spiky, bursting channel activity typical of the Aβ peptide. In figure 24 B, we added zinc within the first 2 minutes of the trace shown and we began to see a decrease in the conductance level of the activity. In figure 24 C, the activity appears to be inhibited by zinc, other than two events, for 10 minutes. Similarly, figure 24 D shows no channel activity due to zinc inhibition for an additional 10 minutes, totaling 20 minutes of channel inhibition likely due to zinc. For the traces shown in figures 24 A-C we applied a constant voltage of 70 mV, while in figure 24 D we applied a constant voltage of -50 mV showing that channel inactivity was not voltage dependent.

We did not expect Aβ42-D1C to show such low and sparse activity given that the amino acids in the 1 to 16 positions of Aβ42 have been suggested to be highly mobile and have poorly defined structures. The Wetzel group also studied cysteine mutagenesis of Aβ40 amyloid fibrils for the N terminus (starting at F4) and found that, similar to the C-terminus findings, these residues in the fibril state were accessible to alkylation and did have significant effects on the fibril stability [69]. Interestingly, we saw visual aggregates in residual samples of Aβ42-D1C (as we did for the Aβ42-A42C mutant). Even though our own observations of fibril formations of the D1C mutant and the results presented by Shivaprasad et al 2005 [69] suggest that this mutant should form oligomeric species, our experimental results thus far found that this mutant has a high tendency towards inactivity. Our study shows that Aβ fibril formation does not necessarily correlate with channel activity.

The replacement of aspartic acid, a charged amino acid, with cysteine, a hydrophobic amino acid, is the most dramatic in terms of hydrophobicity for all the Cys-mutations studied in this work (F and A are both hydrophobic). One of the intended goals for the D1C and A42C mutations was to label the Aβ peptides for single molecule TERF. The results presented here suggest that channel activity in DOPS/DOPE bilayers is sensitive to substitutions in either the N or C termini. Multiple studies have used Aβ peptides labeled on the N terminus. Studies aimed at addressing Aβ channel behavior or other mechanisms of action in combination with reacted probes should take into account our current finding. In spite of our fifteen repeated experiments, the result is currently inconclusive as Aβ42-D1C does not present a clear and constant trend like the one observed for the F19P substitution. Unfortunately, many more experiments would be necessary to obtain a clear description of Aβ42-D1C behavior.

4. CONCLUSIONS

Studying Aβ channel activity of mutated variants has provided valuable insight to structural aspects of the Aβ channel structure. The evidence in this thesis suggests that the Aβ42 C terminus with a U-turn conformation is necessary for membrane insertion. It is still unclear how the Aβ peptide inserts into the membrane.

The inability of the Aβ42-F19P mutant to form ion channels has a clear implication in the structural significance for the F19 residue. The fact that Aβ42-F19P has been shown not to form fibers provides further information into the structural significance of this residue [53, 87, 88]. The lack of activity for Aβ42-F19P suggests that for a stable peptide insertion of channel formation, a β-sheet structure is needed between residues 17-42 in Aβ42. The results with F19P become a control of the "unattractive" activity of Aβ42 and suggest that activity is not the result of unspecific membrane perturbation by the peptide. While this conclusion is only valid for folded and painted bilayers and with the electrolyte used in this study, it is reasonable to predict a similar result for other lipid compositions in which Aβ42 exhibits activity.

One question that might be raised about our results for Aβ42-F19P is why do we not see activity? Perhaps this peptide does not insert or bind to the membrane. It is also possible that this peptide binds and inserts itself into the membrane, but does not form channel structures. Yet, we did observe and calculate minor channel conductance in one experiment. This conclusion does not carry great weight as this activity was seen in *only* 100 seconds in more than 40 hours of recording, yet we did not see similar activity for membrane only experiments. These results allowed us to suggest that, like p3-F19P, Aβ42-F19P might form a collapsed pore that is non-conductive.

Nonetheless, AFM results showed channel-like structures when F19P is reconstituted in bilayers suggesting that Aβ42-F19P has the capability of forming a collapsed pore. Experiments with AFM are ongoing. These results give supporting evidence to the proposed U-turn model for Aβ42 in bilayers.

We showed that Aβ42-F20C forms ion channels and that this activity can be inhibited by millimolar concentrations of zinc. Cysteine residues have a reactive sulfhydryl group and in the future we would like to react the F20C mutant with an MTS reagent once Aβ42-F20C ion channels are formed. It is likely that performing these experiments using painted bilayers would afford more sustained channel activity (ideally as in figure 4). By performing such an experiment we would be able to experimentally determine if the F20 residue lines the pore of the ion channel and directly test the C terminus hairpin model for Aβ channels in a bilayer. This was our original intent for all other cysteine mutations (Aβ42-A42C and Aβ42-D1C); however, because of the lack of sustained activity we found that the N and C termini could be more structurally significant than we originally thought. The second turn in the C terminus of Aβ42, as presented in the model proposed by Strodel et al 2010 [77], could explain why the Aβ42-A42C mutant had such a strong effect on ion channel activity, namely the near lack of step-like and/or bursting activity. Our unexpected results with Aβ42-D1C make evident that the N terminus of Aβ42 must be studied more thoroughly in regards to channel formation. Particularly, critical studies of N terminus mutants are necessary as it is the common location for fluorescently labeling Aβ peptides. This also might point to whether the N terminus is in the path of the channel. Future investigations of single amino acidic mutants on The N and C termini will refine proposed models of Aβ channel structures.

Thus, this work demonstrates the usefulness of functionally studying Aβ mutants and contributes to the understanding of the structural requirements for channel formation and modulation.

The work presented in this thesis suggests that Aβ forms ion channels in the membrane that could cause an imbalance in extracellular and intracellular ionic concentrations, leading to cell death [5, 6, 15, 16, 19-21, 40-46, 49, 50, 71-74]. Moving forward with our research, we would like to test whether a mixture of the wild type and the F19P mutant of Aβ would show ion channel activity or its inhibition. We predict no channel activity with such a mixture as the F19P mutant has such strong tendency to disrupt the channel structure. We would also like to test other Aβ42 mutants. For mutations on the N terminus we might consider replacing D1 with another negatively charged amino acid, glutamic acid (E), as opposed to the dramatic change imposed by the D1C mutant studied in this thesis. Other cysteine mutants might include F4C and M35C as they have been predicted to form fibrils normally, like the F20C mutant. Further cysteine mutants would aid the goal of determining the pore structure of the Aβ channel. The F4C mutant would be a good candidate to give valuable insight into role of the N terminus in Aβ channel structure, while with the M35C mutant we would be able to provide information regarding the C terminus and structural core of the Aβ channel. By comprehensively studying Aβ mutants we believe that it is possible to develop a clear picture of Aβ channel structure.

The present work has clearly demonstrated that the use of Aβ mutants for obtaining structural information of the Aβ channel, although experimentally difficult it is possible.

APPENDIX A: DEFINITIONS OF β SHEET STRUCTURES

Amino acids in proteins and peptides form various secondary structures. In this thesis, the main structure discussed is β sheet (or β pleated sheet). The β sheet involves hydrogen bonding between backbone residues in adjacent chains. They are typical depicted as wide arrows: the tail representing the N-terminus and the head the C-terminus. These β sheets are made up of two or more continuous chains of amino acids that adopt an extended conformation (figure 25 A). The β strands form hydrogen bonds in the backbone with its neighboring β strands, particularly, the bonds form between the donor (amide group) and the acceptor (the carbonyl group) atoms. β sheets can have two orientations: either parallel or antiparallel β strands. The parallel β sheet involves the alignment of the N-termini, while the antiparallel β sheet has the N-terminus of one β strand aligned with the C- terminus of another (figure 25 B and C).

In this thesis, there are two specific structural motifs that β sheets are capable of adopting. The first is the β hairpin (figure 25 D). The β hairpin is the simplest structural motif involving two β strands. The β strands in the β hairpin by definition have an antiparallel arrangement. The second structural motif discussed is the β barrel (figure 25 E). A β barrel is a large, closed form β sheet in which the first strand is hydrogen bonded to the last. β barrel structures are commonly found in proteins that span bacterial cell membranes. In many cases, the strands contained in the β barrel alternate polar and hydrophobic amino acids, aligning in the membrane such that hydrophobic residues are oriented toward the hydrophobic hydrocarbon chains, and hydrophilic residues are oriented toward the interior pore. In this thesis, a β barrel is mentioned in the context of

several Aβ monomers arranging to form an annular structure (such as the ones presented in figure 6, 7, and 8).

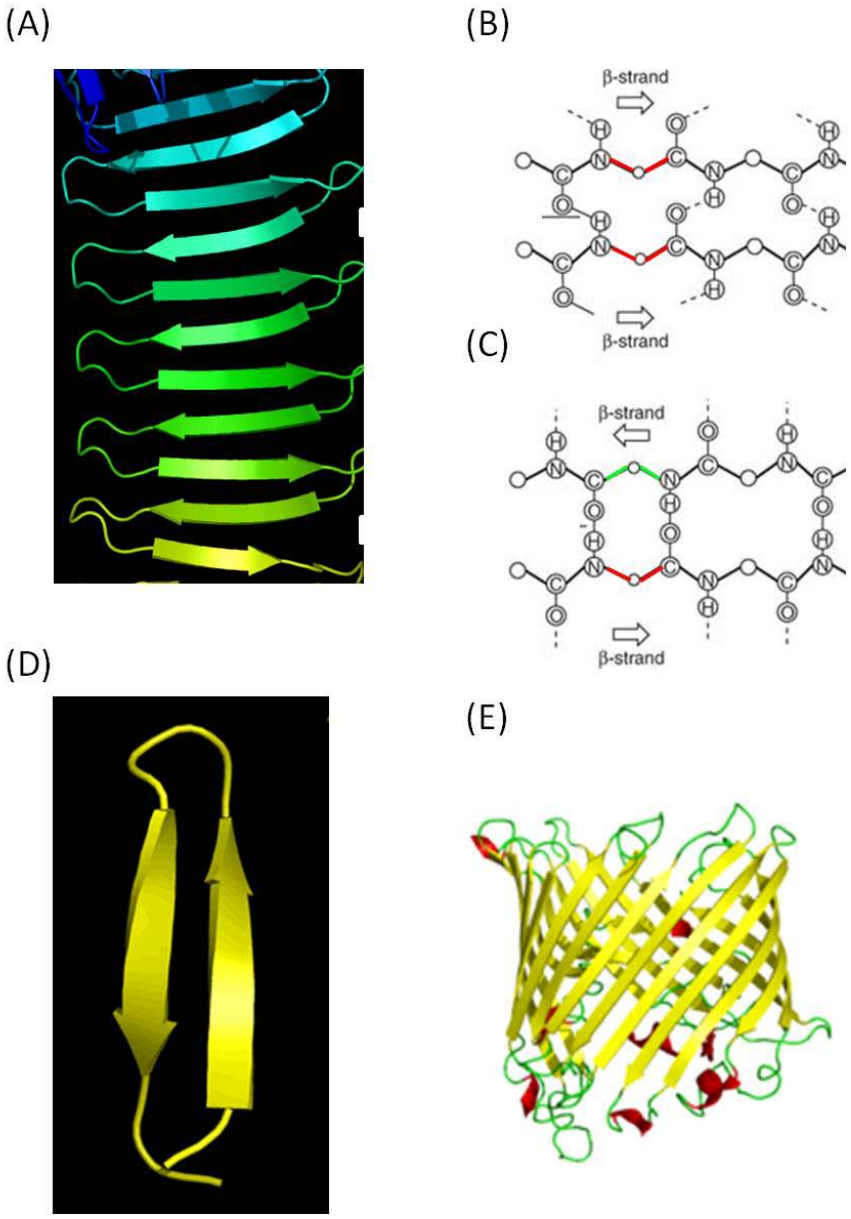

Figure 25: β sheet arrangements and definitions. (A) Example of extended β sheet composed of eleven β strands. The β sheet can be arranged in either (B) parallel or (C) antiparallel. The example shown in panel A is an antiparallel β sheet structure. (D) A single β hairpin structure is composed of two antiparallel strands joined by a loop (i.e. strand-turn-strand motif, PDB: 1fuo). (E) A porin, a single polypeptide, arranged in an antiparallel β barrel structure (PDB ID 1A0S). Images in panel A is taken from Mike Tyka, University of Washington.

REFERENCES

1. Selkoe, D.J., The molecular pathology of Alzheimer's disease. Neuron, 1991. 6(4): p. 487-98.

2. Selkoe, D.J., Amyloid beta protein precursor and the pathogenesis of Alzheimer's disease. Cell, 1989. 58(4): p. 611-2.

3. Selkoe, D.J., Aging, amyloid, and Alzheimer's disease. N Engl J Med, 1989. 320(22): p. 1484-7.

4. Kagan, B.L., R. Azimov, and R. Azimova, Amyloid peptide channels. J Membr Biol, 2004. 202(1): p. 1-10.

5. Kagan, B.L., et al., The channel hypothesis of Huntington's disease. Brain Res Bull, 2001. 56(3-4): p. 281-4.

6. Kagan, B.L., et al., The channel hypothesis of Alzheimer's disease: current status. Peptides, 2002. 23(7): p. 1311-5.

7. Kyle, R.A., Amyloidosis: a convoluted story. Br J Haematol, 2001. 114(3): p. 529-38.

8. Kagan, Bruce L., Antimicrobial Amyloids? Biophysical Journal, 2011. 100(7): p. 1597-1598.

9. Joachim, C.L., H. Mori, and D.J. Selkoe, Amyloid beta-protein deposition in tissues other than brain in Alzheimer's disease. Nature, 1989. 341(6239): p. 226-30.

10. Gillmore, J.D., P.N. Hawkins, and M.B. Pepys, Amyloidosis: a review of recent diagnostic and therapeutic developments. Br J Haematol, 1997. 99(2): p. 245-56.

11. Tan, S.Y., M.B. Pepys, and P.N. Hawkins, Treatment of amyloidosis. Am J Kidney Dis, 1995. 26(2): p. 267-85.

12. Jang, H., et al., Antimicrobial protegrin-1 forms amyloid-like fibrils with rapid kinetics suggesting a functional link. Biophys J, 2011. 100(7): p. 1775-83.

13. Jang, H., et al., Truncated -amyloid peptide channels provide an alternative mechanism for Alzheimer's Disease and Down syndrome. Proceedings of the National Academy of Sciences, 2010. 107(14): p. 6538-6543.

14. Jang, H., et al., Structural convergence among diverse, toxic beta-sheet ion channels. J Phys Chem B, 2010. 114(29): p. 9445-51.

15. Lal, R., H. Lin, and A. Quist, Amyloid beta ion channel: 3D structure and relevance to amyloid channel paradigm. Biochimica et Biophysica Acta (BBA) - Biomembranes, 2007. 1768(8): p. 1966-1975.

16. Lin, H., R. Bhatia, and R. Lal, Amyloid beta protein forms ion channels: implications for Alzheimer's disease pathophysiology. FASEB J, 2001. 15(13): p. 2433-44.

17. Lin, H., Y.J. Zhu, and R. Lal, Amyloid beta protein (1-40) forms calcium-permeable, Zn2+-sensitive channel in reconstituted lipid vesicles. Biochemistry, 1999. 38(34): p. 11189-96.

18. Mustata, M., et al., K3 fragment of amyloidogenic beta(2)-microglobulin forms ion channels: implication for dialysis related amyloidosis. J Am Chem Soc, 2009. 131(41): p. 14938-45.

19. Parbhu, A., et al., Imaging real-time aggregation of amyloid beta protein (1-42) by atomic force microscopy. Peptides, 2002. 23(7): p. 1265-70.

20. Rhee, S.K., A.P. Quist, and R. Lal, Amyloid beta protein-(1-42) forms calcium-permeable, Zn2+-sensitive channel. J Biol Chem, 1998. 273(22): p. 13379-82.

21. Zhu, Y.J., H. Lin, and R. Lal, Fresh and nonfibrillar amyloid beta protein(1-40) induces rapid cellular degeneration in aged human fibroblasts: evidence for AbetaP-channel-mediated cellular toxicity. FASEB J, 2000. 14(9): p. 1244-54.

22. Quist, A., Amyloid ion channels: A common structural link for protein-misfolding disease. Proceedings of the National Academy of Sciences, 2005. 102(30): p. 10427-10432.

23. Hardy, J., The Amyloid Hypothesis of Alzheimer's Disease: Progress and Problems on the Road to Therapeutics. Science, 2002. 297(5580): p. 353-356.

24. Jakob-Roetne, R. and H. Jacobsen, Alzheimer's Disease: From Pathology to Therapeutic Approaches. Angewandte Chemie International Edition, 2009. 48(17): p. 3030-3059.

25. O'Brien, R.J. and P.C. Wong, Amyloid Precursor Protein Processing and Alzheimers Disease. Annu Rev Neurosci, 2010.

26. Yates, D., The molecular pathology of Alzheimer’s disease. Psychiatry, 2008. 7(1): p. 1-5.

27. Capone, R., et al., Amyloid-β-Induced Ion Flux in Artificial Lipid Bilayers and Neuronal Cells: Resolving a Controversy. Neurotoxicity Research, 2009. 16(1): p. 1-13.

28. Choi, J.S., et al., Design of small molecules that target metal-A{beta} species and regulate metal-induced A{beta} aggregation and neurotoxicity. Proc Natl Acad Sci U S A, 2010. 107(51): p. 21990-5.

29. 2011 Alzheimer's Disease Facts and Figures. 2011 [cited 2011 April 16]; Available from: http://www.alz.org/downloads/Facts_Figures_2011.pdf.

30. Healthy Brain vs. Alzheimer Brain. Alzheimer's Association Brain Tour 2011 [cited 2011 April 16]; Available from: http://www.alz.org/brain/09.asp.

31. Thinakaran, G. and E.H. Koo, Amyloid precursor protein trafficking, processing, and function. J Biol Chem, 2008. 283(44): p. 29615-9.

32. Zhang, Y.W., et al., APP processing in Alzheimer's disease. Mol Brain, 2011. 4: p. 3.

33. Nilsberth, C., et al., The 'Arctic' APP mutation (E693G) causes Alzheimer's disease by enhanced Abeta protofibril formation. Nat Neurosci, 2001. 4(9): p. 887-93.

34. Selkoe, D.J., Alzheimer's disease. In the beginning. Nature, 1991. 354(6353): p. 432-3.

35. Haass, C., A.Y. Hung, and D.J. Selkoe, Processing of beta-amyloid precursor protein in microglia and astrocytes favors an internal localization over constitutive secretion. J Neurosci, 1991. 11(12): p. 3783-93.

36. Joachim, C.L., J.H. Morris, and D.J. Selkoe, Diffuse senile plaques occur commonly in the cerebellum in Alzheimer's disease. Am J Pathol, 1989. 135(2): p. 309-19.

37. Selkoe, D.J., Biochemistry of altered brain proteins in Alzheimer's disease. Annu Rev Neurosci, 1989. 12: p. 463-90.

38. Wolfe, M.S. and D.J. Selkoe, Giving Alzheimer's the Old One-Two. Cell, 2010. 142(2): p. 194-196.

39. Capone, R., et al., Antimicrobial Protegrin-1 Forms Ion Channels: Molecular Dynamic Simulation, Atomic Force Microscopy, and Electrical Conductance Studies. Biophysical Journal, 2010. 98(11): p. 2644-2652.

40. Arispe, N., H.B. Pollard, and E. Rojas, Giant multilevel cation channels formed by Alzheimer disease amyloid beta-protein [A beta P-(1-40)] in bilayer membranes. Proc Natl Acad Sci U S A, 1993. 90(22): p. 10573-7.

41. Arispe, N., H.B. Pollard, and E. Rojas, The ability of amyloid beta-protein [A beta P (1-40)] to form Ca2+ channels provides a mechanism for neuronal death in Alzheimer's disease. Ann N Y Acad Sci, 1994. 747: p. 256-66.

42. Arispe, N., H.B. Pollard, and E. Rojas, beta-Amyloid Ca(2+)-channel hypothesis for neuronal death in Alzheimer disease. Mol Cell Biochem, 1994. 140(2): p. 119-25.

43. Arispe, N., E. Rojas, and H.B. Pollard, Alzheimer disease amyloid beta protein forms calcium channels in bilayer membranes: blockade by tromethamine and aluminum. Proc Natl Acad Sci U S A, 1993. 90(2): p. 567-71.

44. Durell, S.R., et al., Theoretical models of the ion channel structure of amyloid beta-protein. Biophys J, 1994. 67(6): p. 2137-45.

45. Pollard, H.B., E. Rojas, and N. Arispe, A new hypothesis for the mechanism of amyloid toxicity, based on the calcium channel activity of amyloid beta protein (A beta P) in phospholipid bilayer membranes. Ann N Y Acad Sci, 1993. 695: p. 165-8.

46. Pollard, J.R., et al., A geometric sequence that accurately describes allowed multiple conductance levels of ion channels: the "three-halves (3/2) rule". Biophys J, 1994. 67(2): p. 647-55.

47. Hirakura, Y. and B.L. Kagan, Pore formation by beta-2-microglobulin: a mechanism for the pathogenesis of dialysis associated amyloidosis. Amyloid, 2001. 8(2): p. 94-100.

48. Hirakura, Y., M.C. Lin, and B. Kagan, Erratum: hirakura Y, lin M-C, kagan BL. 1999. Alzheimer amyloid Abeta1-42 channels: effects of solvent, pH, and congo red. J neurosci res 57:458-466. J Neurosci Res, 1999. 58(5): p. 726.

49. Hirakura, Y., M.C. Lin, and B.L. Kagan, Alzheimer amyloid abeta1-42 channels: effects of solvent, pH, and Congo Red. J Neurosci Res, 1999. 57(4): p. 458-66.

50. Lin, M.C. and B.L. Kagan, Electrophysiologic properties of channels induced by Abeta25-35 in planar lipid bilayers. Peptides, 2002. 23(7): p. 1215-28.

51. Hardy, J.A. and G.A. Higgins, Alzheimer's disease: the amyloid cascade hypothesis. Science, 1992. 256(5054): p. 184-5.

52. Cannon, M.J., et al., Kinetic analysis of beta-amyloid fibril elongation. Anal Biochem, 2004. 328(1): p. 67-75.

53. Williams, A.D., et al., Mapping abeta amyloid fibril secondary structure using scanning proline mutagenesis. J Mol Biol, 2004. 335(3): p. 833-42.

54. Williams, T.L., I.J. Day, and L.C. Serpell, The Effect of Alzheimer's Aβ Aggregation State on the Permeation of Biomimetic Lipid Vesicles. Langmuir, 2010. 26(22): p. 17260-17268.

55. Wogulis, M., Nucleation-Dependent Polymerization Is an Essential Component of Amyloid-Mediated Neuronal Cell Death. Journal of Neuroscience, 2005. 25(5): p. 1071-1080.

56. Ryu, J., et al., Inhibition of β-amyloid peptide aggregation and neurotoxicity by α-d-mannosylglycerate, a natural extremolyte. Peptides, 2008. 29(4): p. 578-584.

57. Ban, T., et al., Direct Observation of Aβ Amyloid Fibril Growth and Inhibition. Journal of Molecular Biology, 2004. 344(3): p. 757-767.

58. Balbach, J.J., et al., Amyloid fibril formation by A beta 16-22, a seven-residue fragment of the Alzheimer's beta-amyloid peptide, and structural characterization by solid state NMR. Biochemistry, 2000. 39(45): p. 13748-59.

59. Wang, Z., AFM and STM study of β-amyloid aggregation on graphite. Ultramicroscopy, 2003. 97(1-4): p. 73-79.

60. Ferretti, M.T., et al., Intracellular Abeta-oligomers and early inflammation in a model of Alzheimer's disease. Neurobiol Aging, 2011.

61. Klein, W.L., Abeta toxicity in Alzheimer's disease: globular oligomers (ADDLs) as new vaccine and drug targets. Neurochem Int, 2002. 41(5): p. 345-52.

62. Umeda, T., et al., Intraneuronal amyloid beta oligomers cause cell death via endoplasmic reticulum stress, endosomal/lysosomal leakage, and mitochondrial dysfunction in vivo. J Neurosci Res, 2011. 89(7): p. 1031-42.

63. Arispe, N. and M. Doh, Plasma membrane cholesterol controls the cytotoxicity of Alzheimer's disease AbetaP (1-40) and (1-42) peptides. FASEB J, 2002. 16(12): p. 1526-36.

64. Simakova, O. and N.J. Arispe, Early and late cytotoxic effects of external application of the Alzheimer's Abeta result from the initial formation and function of Abeta ion channels. Biochemistry, 2006. 45(18): p. 5907-15.

65. Bhatia, R., H. Lin, and R. Lal, Fresh and globular amyloid beta protein (1-42) induces rapid cellular degeneration: evidence for AbetaP channel-mediated cellular toxicity. FASEB J, 2000. 14(9): p. 1233-43.

66. Jarrett, J.T., E.P. Berger, and P.T. Lansbury, Jr., The C-terminus of the beta protein is critical in amyloidogenesis. Ann N Y Acad Sci, 1993. 695: p. 144-8.

67. Jarrett, J.T., E.P. Berger, and P.T. Lansbury, Jr., The carboxy terminus of the beta amyloid protein is critical for the seeding of amyloid formation: implications for the pathogenesis of Alzheimer's disease. Biochemistry, 1993. 32(18): p. 4693-7.

68. Jarrett, J.T. and P.T. Lansbury, Jr., Seeding "one-dimensional crystallization" of amyloid: a pathogenic mechanism in Alzheimer's disease and scrapie? Cell, 1993. 73(6): p. 1055-8.

69. Shivaprasad, S. and R. Wetzel, Scanning cysteine mutagenesis analysis of Abeta-(1-40) amyloid fibrils. J Biol Chem, 2006. 281(2): p. 993-1000.

70. Stine, W.B., Jr., et al., In vitro characterization of conditions for amyloid-beta peptide oligomerization and fibrillogenesis. J Biol Chem, 2003. 278(13): p. 11612-22.

71. Mirzabekov, T., et al., Channel formation in planar lipid bilayers by a neurotoxic fragment of the beta-amyloid peptide. Biochem Biophys Res Commun, 1994. 202(2): p. 1142-8.

72. Arispe, N., et al., Polyhistidine Peptide Inhibitor of the Aβ Calcium Channel Potently Blocks the Aβ-Induced Calcium Response in Cells. Theoretical Modeling Suggests a Cooperative Binding Process. Biochemistry, 2010. 49(36): p. 7847-7853.

73. Shafrir, Y., et al., Models of membrane-bound Alzheimer's Abeta peptide assemblies. Proteins, 2010. 78(16): p. 3473-87.

74. Shafrir, Y., et al., Beta-barrel models of soluble amyloid beta oligomers and annular protofibrils. Proteins: Structure, Function, and Bioinformatics, 2010. 78(16): p. 3458-3472.

75. Ma, B. and R. Nussinov, Molecular dynamics simulations of alanine rich beta-sheet oligomers: Insight into amyloid formation. Protein Sci, 2002. 11(10): p. 2335-50.

76. Ma, B. and R. Nussinov, Stabilities and conformations of Alzheimer's beta - amyloid peptide oligomers (Abeta 16-22, Abeta 16-35, and Abeta 10-35): Sequence effects. Proc Natl Acad Sci U S A, 2002. 99(22): p. 14126-31.

77. Strodel, B., et al., Transmembrane structures for Alzheimer's Abeta(1-42) oligomers. J Am Chem Soc, 2010. 132(38): p. 13300-12.

78. Petkova, A.T., et al., A structural model for Alzheimer's beta -amyloid fibrils based on experimental constraints from solid state NMR. Proc Natl Acad Sci U S A, 2002. 99(26): p. 16742-7.

79. Benzinger, T.L., et al., Propagating structure of Alzheimer's beta-amyloid(10-35) is parallel beta-sheet with residues in exact register. Proc Natl Acad Sci U S A, 1998. 95(23): p. 13407-12.

80. Fraser, P.E., et al., Conformation and fibrillogenesis of Alzheimer A beta peptides with selected substitution of charged residues. J Mol Biol, 1994. 244(1): p. 64-73.

81. Jang, H., et al., Transmembrane β-Barrel Topology Model for Alzheimer's β-Amyloid (Aβ) Ion Channels. Biophys J, 2011. 100(3): p. 201a-201a.

82. Montal, M. and P. Mueller, Formation of bimolecular membranes from lipid monolayers and a study of their electrical properties. Proc Natl Acad Sci U S A, 1972. 69(12): p. 3561-6.

83. Mayer, M., et al., Microfabricated teflon membranes for low-noise recordings of ion channels in planar lipid bilayers. Biophys J, 2003. 85(4): p. 2684-95.

84. Capone, R., et al., Designing nanosensors based on charged derivatives of gramicidin A. J Am Chem Soc, 2007. 129(31): p. 9737-45.

85. Molleman, A., Patch Clamping: An Introductory Guide to Patch Clamp Electrophysiology. 2003, John Wiley and Sons Ltd.

86. Kourie, J.I., C.L. Henry, and P. Farrelly, Diversity of amyloid beta protein fragment [1-40]-formed channels. Cell Mol Neurobiol, 2001. 21(3): p. 255-84.

87. Wood, S.J., et al., Prolines and amyloidogenicity in fragments of the Alzheimer's peptide beta/A4. Biochemistry, 1995. 34(3): p. 724-30.

88. Moriarty, D.F. and D.P. Raleigh, Effects of sequential proline substitutions on amyloid formation by human amylin20-29. Biochemistry, 1999. 38(6): p. 1811-8.

89. Morimoto, A., et al., Aggregation and neurotoxicity of mutant amyloid beta (A beta) peptides with proline replacement: importance of turn formation at positions 22 and 23. Biochem Biophys Res Commun, 2002. 295(2): p. 306-11.